

## NRC Publications Archive Archives des publications du CNRC

### **Mixed lipopeptide-based mucosal vaccine candidate induces cross-variant immunity and protects against SARS-CoV-2 infection in hamsters**

Patel, Raj S.; Duque, Diana; Bavananthasivam, Jegarubee; Hewitt, Melissa; Sandhu, Jagdeep K.; Kumar, Rakesh; Tran, Anh; Agrawal, Babita

This publication could be one of several versions: author's original, accepted manuscript or the publisher's version. / La version de cette publication peut être l'une des suivantes : la version prépublication de l'auteur, la version acceptée du manuscrit ou la version de l'éditeur.

For the publisher's version, please access the DOI link below. / Pour consulter la version de l'éditeur, utilisez le lien DOI ci-dessous.

#### **Publisher's version / Version de l'éditeur:**

<https://doi.org/10.1093/immhor/vlae011>

*ImmunoHorizons*, 9, 2, 2025-01-24

#### **NRC Publications Archive Record / Notice des Archives des publications du CNRC :**

<https://nrc-publications.canada.ca/eng/view/object/?id=23288a6d-f180-49bb-a36c-a848f52c754e>

<https://publications-cnrc.canada.ca/fra/voir/objet/?id=23288a6d-f180-49bb-a36c-a848f52c754e>

Access and use of this website and the material on it are subject to the Terms and Conditions set forth at

<https://nrc-publications.canada.ca/eng/copyright>

READ THESE TERMS AND CONDITIONS CAREFULLY BEFORE USING THIS WEBSITE.

L'accès à ce site Web et l'utilisation de son contenu sont assujettis aux conditions présentées dans le site

<https://publications-cnrc.canada.ca/fra/droits>

LISEZ CES CONDITIONS ATTENTIVEMENT AVANT D'UTILISER CE SITE WEB.

**Questions?** Contact the NRC Publications Archive team at

PublicationsArchive-ArchivesPublications@nrc-cnrc.gc.ca. If you wish to email the authors directly, please see the first page of the publication for their contact information.

**Vous avez des questions?** Nous pouvons vous aider. Pour communiquer directement avec un auteur, consultez la première page de la revue dans laquelle son article a été publié afin de trouver ses coordonnées. Si vous n'arrivez pas à les repérer, communiquez avec nous à PublicationsArchive-ArchivesPublications@nrc-cnrc.gc.ca.

# Mixed lipopeptide-based mucosal vaccine candidate induces cross-variant immunity and protects against SARS-CoV-2 infection in hamsters

Raj S. Patel<sup>1</sup>, Diana Duque<sup>2</sup>, Jegarubee Bavananthasivam<sup>2</sup>, Melissa Hewitt<sup>3</sup>, Jagdeep K. Sandhu <sup>3</sup>, Rakesh Kumar<sup>4</sup>, Anh Tran <sup>2,5</sup>, and Babita Agrawal<sup>1,\*</sup>

<sup>1</sup>Department of Surgery, Faculty of Medicine and Dentistry, College of Health Sciences, University of Alberta, Edmonton, AB, Canada

<sup>2</sup>Infectious Diseases, Human Health Therapeutics Research Centre, National Research Council Canada, Ottawa, ON, Canada

<sup>3</sup>Preclinical Imaging, Human Health Therapeutics Research Centre, National Research Council Canada, Ottawa, ON, Canada

<sup>4</sup>ImMed Biotechnologies, Edmonton, AB, Canada

<sup>5</sup>Department of Biochemistry, Microbiology and Immunology, University of Ottawa, Ottawa, ON, Canada

\*Corresponding author: University of Alberta, 720 Heritage Medical Research Centre, 11207 - 87 Ave NW, Edmonton AB, T6G 2S2, Canada.  
Email: bagrawal@ualberta.ca.

## Abstract

The global dissemination of SARS-CoV-2 led to a worldwide pandemic in March 2020. Even after the official downgrading of the COVID-19 pandemic, infection with SARS-CoV-2 variants continues. The rapid development and deployment of SARS-CoV-2 vaccines helped to mitigate the pandemic to a great extent. However, the current vaccines are suboptimal; they elicit incomplete and short-lived protection and are ineffective against evolving virus variants. Updating the spike antigen according to the prevailing variant and repeated boosters is not the long-term solution. We have designed a lipopeptide-based, mucosal, pan-coronavirus vaccine candidate, derived from highly conserved and/or functional regions of the SARS-CoV-2 spike, nucleocapsid, and membrane proteins. Our studies demonstrate that the designed lipopeptides (LP<sub>Mix</sub>) induced both cellular and humoral (mucosal and systemic) immune responses upon intranasal immunization in mice. Furthermore, the antibodies bound to the wild-type and mutated S proteins of SARS-CoV-2 variants of concern, including Alpha, Beta, Delta and Omicron, and also led to efficient neutralization in a surrogate viral neutralization assay. Our sequence alignment and 3-dimensional molecular modeling studies demonstrated that spike-derived epitopes, P<sub>1</sub> and P<sub>2</sub>, are sequentially and/or structurally conserved among the SARS-CoV-2 variants. The addition of a novel mucosal adjuvant, heat-killed *Caulobacter crescentus*, to the lipopeptide vaccine significantly bolstered mucosal antibody responses. Finally, the lipopeptide-based intranasal vaccine demonstrated significant improvement in lung pathologies in a hamster model of SARS-CoV-2 infection. These studies are fundamentally important and open new avenues in the investigation of an innovative, broadly protective intranasal vaccine platform for SARS-CoV-2 and its variants.

**Keywords:** conserved epitopes, humoral/cellular immunity, next-generation COVID-19 vaccines, pan-coronavirus, SARS-CoV-2

## Introduction

As the global community transitions out of the COVID-19 pandemic, vaccine strategies against SARS-CoV-2 must shift to implementing long-term, proactive measures to prevent future infections and outbreaks. To date, BNT162b2 (Pfizer-BioNTech) and mRNA-1273 (Moderna) have been the most widely used vaccines against SARS-CoV-2.<sup>1</sup> Compared with conventional vaccines, the messenger RNA (mRNA)-based lipid nanoparticle vaccines were safe; showed vaccine efficacies exceeding 94%; and protected against mortalities, hospitalizations, and severe disease outcomes, and their remarkable scalability was ideal for implementing during a public health emergency.<sup>1</sup> However, current vaccines do not prevent infections and despite these vaccination efforts, SARS-CoV-2 infections have continued to rise. As of March 2024, SARS-CoV-2 has infected more than 772 million people and caused over 7 million deaths worldwide.<sup>2</sup> Breakthrough infections raise serious concerns about vaccine efficacies and their susceptibility to novel SARS-CoV-2 variants of concern (VOCs), thereby increasing the need for next-generation vaccine strategies.<sup>3,4</sup> Current practices of periodically updating vaccines have shown to be time-consuming, costly, and compromised in efficacy, and offer a temporary solution to a long-term problem.<sup>1</sup> Therefore,

it is necessary to develop a vaccine that enhances protection against multiple SARS-CoV-2 variants and a broader class of coronavirus, prevents infections, and elicits durable, long-lasting immunity.

Beyond mRNA vaccines, there are several different vaccine technologies currently being tested for COVID-19, including ZyCoV-D (DNA based), Novavax Nuvaxovid (protein based), Covaxin BBV152 (whole virion inactivated), and Vaxzevria (viral vector based), the majority of which are administered intramuscularly.<sup>1</sup> The lack of mucosal immunity induced by intramuscular immunizations leaves individuals vulnerable to SARS-CoV-2 infections, and requires researchers to explore alternative routes of administration, including intranasal. To date, 4 intranasal vaccines have been approved for COVID-19, including RAZI-COV PARS (Razi Vaccine), iNCOVACC (Bharat Biotech), Convidecia Air (CanSino Biologics), and Gam-COVID-Vac (Gamaleya National Center), all of which are aerosolized versions of approved intramuscular vaccines.<sup>5–8</sup> Despite these advancements, the development of an optimal vaccine platform and adjuvant remains elusive. Interestingly, lipopeptide-based vaccines offer a potential advantage for establishing both mucosal and systemic immunity through intranasal immunizations.<sup>9</sup>

Received: November 7, 2024. Accepted: November 14, 2024

© The Author(s) 2025. Published by Oxford University Press on behalf of The American Association of Immunologists.

This is an Open Access article distributed under the terms of the Creative Commons Attribution-NonCommercial License (<https://creativecommons.org/licenses/by-nc/4.0/>), which permits non-commercial re-use, distribution, and reproduction in any medium, provided the original work is properly cited. For commercial re-use, please contact [journals.permissions@oup.com](mailto:journals.permissions@oup.com)

Lipopeptides demonstrate the ability to self-assemble into micelles, passively cross cell membranes, efficiently deliver peptide antigens to mucosal-associated lymphoid tissues, enhance antigen presentation, and induce systemic as well as mucosal peptide-specific B cells, T helper (Th) cells, and cytotoxic T lymphocytes (CTLs).<sup>9–11</sup> Furthermore, the simplicity of the lipopeptide design provides developing nations and remote jurisdictions accessibility to disease-preventing vaccines which are easily producible, cost-effective, and more stable, with lower storage demands, compared with mRNA vaccines.<sup>1,9,10,12</sup>

Neutralizing antibody (nAbs) responses induced by vaccines and/or natural infections predict protection against SARS-CoV-2 infections to a great extent.<sup>13</sup> The absence of an early nAb response strongly correlates with mortalities and delayed viral control.<sup>14</sup> However, the role of non-neutralizing antibodies in protecting from severe disease cannot be undermined. Convalescent blood from COVID-19 patients with mild disease have shown a higher proportion of nucleocapsid (N)- and membrane (M)-specific T cells, compared with spike (S)-specific cells. This highlights the importance of non-S-specific T cells contributing to protection.<sup>15–17</sup> Furthermore, due to the accumulation of mutations in the S protein, infections with emerging SARS-CoV-2 variants cannot be mitigated solely by nAbs. Therefore, next-generation vaccines need to look beyond nAb titers. The M and N proteins are conserved proteins among coronaviruses and can be potential targets for a pan-coronavirus vaccine.

In this study, we aim to investigate a novel vaccine strategy that could broadly protect against SARS-CoV-2, its variants, and other heterologous coronaviruses. We identified 7 highly conserved, immunodominant epitopes (P<sub>1–7</sub>) derived from the S, N, and M proteins of SARS-CoV-2 shown to be clinically protective B cell, Th cell, and CTL epitopes.<sup>16,18–28</sup> Next, corresponding lipopeptides were synthesized by conjugating a palmitoyl group at the carboxyl terminal for each selected epitope. We previously reported that intranasal immunization of mice with individual lipopeptides induced potent cellular and humoral immune responses against its target antigen.<sup>29</sup> Here, we investigated a lipopeptide mix (LP<sub>Mix</sub>) vaccine formulation that induced broad immunity against multiple antigens of SARS-CoV-2 in animal models. In addition, we incorporated a novel mucosal adjuvant, heat-killed *Caulobacter crescentus* (HKCC), that stimulates the innate immune system, and promotes dendritic cell (DCs) and natural killer (NK)/NK-T cell interactions.<sup>30</sup> Our studies revealed that a 2-dose, intranasal immunization regimen with LP<sub>Mix</sub> induces a robust splenocyte proliferation response and mucosal and systemic cross-reactive IgA/IgM as well as strong nAb titers. Next, our LP<sub>Mix</sub> vaccine formulations, with or without HKCC as an adjuvant, were assessed for effectiveness in protecting against Omicron (BA.5)-infected hamsters. Interestingly, prophylactic immunization with our LP<sub>Mix</sub>-based vaccines induced high nAb titers and significantly improved lung pathology in infected hamsters. In conclusion, these studies endorse the development of our LP<sub>Mix</sub> vaccine candidate as a potential next-generation COVID-19 vaccine.

## Materials and methods

### Synthetic lipopeptides, peptides, and adjuvants

Synthetic lipopeptides [LP<sub>1</sub> (Spike S<sub>1</sub> aa<sub>492–505</sub>): LQSYGFQPTNGVGYK(Palmitoyl)G, LP<sub>2</sub> (Spike S<sub>2</sub> aa<sub>814–826</sub>): KRSFIEDLLFNKVK(Palmitoyl)G, LP<sub>3</sub> (NCAP aa<sub>358–372</sub>): IDAYK

TFPPTPEPKDK(Palmitoyl)G, LP<sub>4</sub> (NCAP aa<sub>317–331</sub>): MSRIGMEVTPSGTWLK (Palmitoyl)G, LP<sub>5</sub> (NCAP aa<sub>158–172</sub>): VLQLPQGTTLPKGFYK(Palmitoyl)G, LP<sub>6</sub> (Mem aa<sub>98–112</sub>): ASFRLFARTRSMWSFK(Palmitoyl)G, and LP<sub>7</sub> (Mem aa<sub>34–48</sub>): LLQFAYANRRNFLYIK(Palmitoyl)G] and their corresponding native peptides (P<sub>1</sub>: LQSYGFQPTNGVGY; P<sub>2</sub>: KRSFIEDLLFNKV; P<sub>3</sub>: IDAYKTFPPTPEPKD; P<sub>4</sub>: MSRIGMEVTPSGTWL; P<sub>5</sub>: VLQLPQGTTLPKGFY; P<sub>6</sub>: ASFRLFARTRSMWSF; and P<sub>7</sub>: LLQFAYANRRNFLYI, respectively) were custom synthesized by GenScript with >96% purity.<sup>29</sup> All lipopeptides and peptides were prepared in DMSO at 10 mg/mL, stored at –20 °C, and diluted in phosphate-buffered saline (PBS) or culture media before use. HKCC, an innate immunity stimulant, was used as an adjuvant.<sup>30</sup>

### Heat-killed *C. crescentus*

*C. crescentus* (ATCC; 19089), was grown in an incubator at room temperature (22–27 °C) in PYE medium. Logarithmically growing cultures were centrifuged at 6000 rpm for 15 min and the bacterial colony-forming units was determined by measuring optical density (OD) and confirmed by plating serially diluted bacterial suspensions on PYE agar. To prepare HKCC, live *C. crescentus* was treated at 80 °C for 60 min, centrifuged, and resuspended in saline to desired concentrations. To determine viability after heat treatment, the prepared suspension of HKCC was plated on PYE agar plates in serial dilutions. No bacterial colonies grew in these plates confirming the nonviability of bacterial cells. Every batch of HKCC was tested to confirm nonviability prior to use.

### Mice immunization

Animal experiments were approved by the University of Alberta's Animal Care and Use Committee for Health Sciences and conducted by following the guidelines of the Canadian Council of Animal Care. Four- to 6-wk-old male C57BL/6 mice (purchased from Charles River Laboratories) were housed in a pathogen-free animal facility, Health Sciences Laboratory Animal Services (HSLAS), at the University of Alberta. Mice were acclimatized to the experimental location for 7 d and randomly assigned into treatment groups. Researchers were not blinded to the allocated groups. Mice were immunized twice, 14 d apart, intranasally with a lipopeptide mix vaccine (LP<sub>Mix</sub>: LP<sub>1</sub>, LP<sub>2</sub>, LP<sub>3</sub>, LP<sub>4</sub>, LP<sub>5</sub>, LP<sub>6</sub>, and LP<sub>7</sub>; each LP given at 10 µg/mouse or 1 µg/mouse) in the absence or presence of HKCC adjuvant, under light anesthesia with isoflurane (O<sub>2</sub> flow rate: 0.5–1 L/min with isoflurane vaporizer at 2%–4%) (Fig. 1A and B). Mice were humanely euthanized 7 d after the second immunization by CO<sub>2</sub>. Bronchoalveolar lavages (BALs), sera, lungs, and spleens were collected for analysis (Fig. 1C). Animal experiments were repeated thrice, each with n = 4 to 5 mice per immunization group. Unimmunized mice were used as control animals.

### Antigen-specific splenocytes proliferation assay

Antigen-specific splenocyte proliferation assays were conducted as previously reported.<sup>29</sup> Splenocytes derived from immunization groups were restimulated ex vivo with individual lipopeptides (LP<sub>1–7</sub>) and peptides (P<sub>1–7</sub>) at 0.1 µg/mL as recall antigens. Plates were incubated for 4 d, before adding BrdU labeling solution for 18 h. The levels of BrdU incorporation in proliferating splenocytes were measured using a Roche Cell Proliferation ELISA, BrdU colorimetric kit

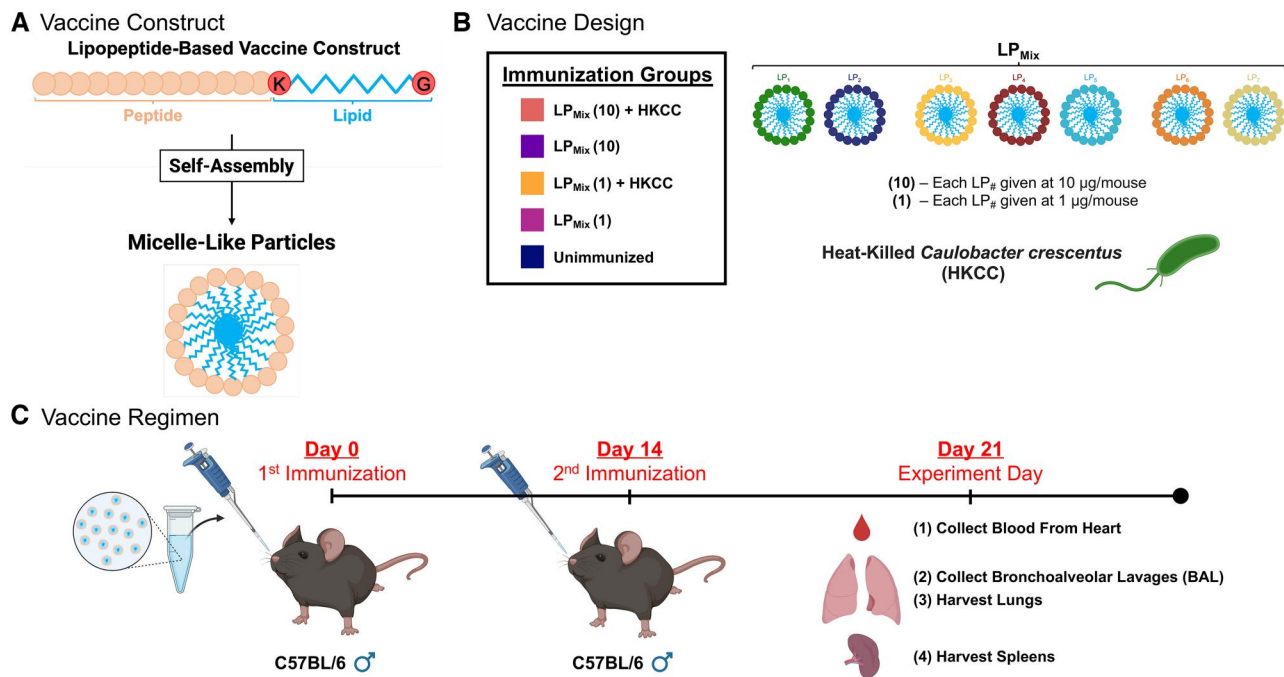


**Figure 1.** Vaccine construct, design, and regimen. (A) Schematic representation of the lipopeptide-based vaccine construct and its physicochemical nature of self-formulating into a micelle-like particle.<sup>29</sup> The lipopeptide-based vaccine construct consists of a peptide (tan) covalently attached with a lysine-palmitoyl-glycine chain (red/blue) at the carboxy terminal. (B) Seven lipopeptides, LP<sub>1-7</sub> (described in the Materials and Methods) were synthesized and mixed to formulate a lipopeptide mix vaccine (LP<sub>Mix</sub>). The LP<sub>Mix</sub> vaccine was tested at 2 doses, in which each LP was given at 10 µg/mouse [LP<sub>Mix</sub>(10)] or 1 µg/mouse [LP<sub>Mix</sub>(1)] in the presence or absence of the HKCC adjuvant. (C) Depiction of the vaccine regimen illustrating the immunization timeline and sample collection in mice. Adapted from Patel & Agrawal.<sup>29</sup>

(Sigma-Aldrich) and counted by a DTX 880 Plate Reader (Beckman Coulter), set at 450 nm. OD readings were acquired, subtracted by APC + splenocytes background, and reported as mean ± SEM of triplicate values.

### Isolation of lung lymphocytes

Lungs were harvested and pooled from 4 to 5 mice. Lung lymphocytes were isolated as previously described.<sup>29</sup>

### Flow cytometry of immune cells

Isolated lung lymphocytes ( $2 \times 10^6$  cells) and splenocytes ( $2 \times 10^6$  cells) from immunized mice were stimulated with PMA (50 ng/mL) and ionomycin (500 ng/mL) for 20 h at 37 °C. Next, brefeldin A (1.5 µg/mL) was added and incubated for 4 h at 37 °C. Subsequently, the lung lymphocytes and splenocytes were stained with a T cell panel (Live/Dead NIR, CD3-Alexa Fluor 488, CD4-BV786, CD8b-BUV615, CCR7-BV650, IFN $\gamma$ -PE, TNF $\alpha$ -BV711, IL-2-BUV737, IL-10-PerCP-Cy5.5, and Foxp3-APC; Thermo Fisher Scientific) and a B cell panel (Live/Dead NIR, CD19-BUV615, CD27-SB600, IgD-PE-Cy7, IgM-SB780, and B.1.617 Spike-APC conjugate; Thermo Fisher Scientific), using an established flow cytometry staining protocol.<sup>31</sup> Samples were run on a Cytex Aurora Spectral Flow Cytometer (Cytex Biosciences) and analyzed by FlowJo v10.10 software (BD). For T cell analysis, splenocytes and lung lymphocyte samples from immunized groups were concatenated to provide consistency in generating t-distributed stochastic neighbor embedding plots and clustering methods. PhenoGraph was used to identify unique immune cell clusters within lung and spleen samples of immunized groups based on phenotypic markers that were expressed.<sup>32</sup> Mean fluorescence intensity (MFI) values were acquired for each phenotypic marker for all clusters, and represented as heatmaps, created by Morpheus.<sup>33</sup>

### Enzyme-linked immunosorbent assay for antigen-specific serum and BAL antibody responses

NUNC MaxiSorp 96-well flat-bottom plates were coated with synthetic lipopeptides (LP<sub>1-7</sub>), peptides (P<sub>1-7</sub>), and SARS-CoV-2 N, M, and S proteins of the Alpha (B.1.1.7), Beta (B.1.351), Delta (B.1.617), and Omicron (BA.1, BA.4, BA.5, BQ1.1, EG.5) variants in individual plates at 1 µg/mL in PBS and stored overnight at 4 °C (GenScript). Next, wells were blocked with buffer (1x PBS + 1% fetal bovine serum) for 1 h at room temperature (RT), followed by the addition of individual serum (1:100, 1:200) and BAL (1:2, 1:4) samples (triplicates) for 2 h at RT. Next, the appropriate secondary antibody, goat anti-mouse IgA-alkaline phosphatase or IgM-alkaline phosphatase (1:4,000; SouthernBiotech), was loaded into each well for 1 h at RT. Next, color development was achieved by adding p-nitrophenyl phosphate (substrate; SouthernBiotech). Plates were read using a DTX 880 Plate Reader (Beckman Coulter) at 405 nm after 1.5 h. IgA and IgM standard curves were performed to interpolate the amounts of antigen-specific IgA and IgM antibody concentrations (µg/mL), respectively. Bars are expressed as the mean (Ig) ± SEM of triplicate wells.

### PyMOL

From the RCSB protein data base, S proteins of the wild-type (6VW1), Alpha (7EKF), Beta (7WEV), Delta (7W98), and Omicron (7T9K) variants were uploaded onto PyMOL. The protein structures of the LP<sub>1</sub> and LP<sub>2</sub> epitopes were visualized. Images were captured as ribbon diagrams and under licorice view to understand the folded 3-dimensional conformation of secondary structures and molecular geometry within the structure. Using the sequence alignment tool, amino acid sequences were compared with identify mutations

in the LP<sub>1</sub> and LP<sub>2</sub> epitopes across multiple SARS-CoV-2 variants.

### Cells and viruses

Vero-TMPRSS2 were maintained in incubators at 37 °C and 5% CO<sub>2</sub>. Cells were maintained in growth medium (Dulbecco's Modified Eagle Medium supplemented with 1X nonessential amino acids, 1 mM sodium pyruvate, and 5% fetal bovine serum was used to maintain the cells).

The SARS-CoV-2 VOC used in hamster challenge study was obtained from BEI Resources: hCoV-19/South Africa/CERI-KRISP-K040013/2022 (lineage BA.5; Omicron variant, NR-56798). SARS-CoV-2 strain was amplified and titered on Vero E6 expressing TMPRSS2. Sanger sequencing of the S gene confirmed genetic identity to original isolate. All in vivo studies used Omicron BA.5 at passage 4.

### Animal study

All hamster studies were conducted at the small animal facility of the National Research Council Canada (NRC) in accordance with the guidelines of the Canadian Council on Animal Care. All procedures performed on hamsters in this study were in accordance with regulations and guidelines reviewed and approved in animal use protocol 2020.06 by the NRC Human Health Therapeutics Animal Care Committee. All SARS-CoV-2 work was done at the NRC's certified small animal biocontainment level 3 facility. Researchers were blinded to the experimental groups.

Animal challenge study was conducted with a total of 23 male Golden Syrian hamsters (81–90 g, 6–7 wk old; Charles River Laboratories). Hamsters were randomly divided into treatment groups. Hamsters were vaccinated with a lipopeptide mix vaccine (LP<sub>Mix</sub>: LP<sub>1</sub>, LP<sub>2</sub>, LP<sub>3</sub>, LP<sub>4</sub>, LP<sub>5</sub>, LP<sub>6</sub>, and LP<sub>7</sub>; each LP given at 10 µg/hamster) in the absence or presence of HKCC adjuvant, under light anesthesia with isoflurane. The treatment groups received 2 vaccination doses on day 24 (D24) and D10 by intranasal route (where day 0 is the day of challenge). Serum was collected on days 14 and 24 post-treatment. Oral swab samples were collected in 600 µL PBS on D3 and D5 postinfection. Immunized hamsters were anesthetized by injection of ketamine and xylazine (90 kg/mg and 8 kg/mg) and intranasally challenged with Omicron BA.5 at 50% tissue culture infectious dose (TCID<sub>50</sub>) of 1.67 × 10<sup>5</sup> per animal. Weight and clinical symptoms were monitored daily. Animals were humanely euthanized by CO<sub>2</sub> at D5 postinfection and tissues immediately collected for analysis.

### Real-time quantitative polymerase chain reaction

Genomic viral RNA was quantified as previously described.<sup>34</sup> Briefly, viral RNA from hamster respiratory tissues including lung and nasal turbinate were extracted using Quick-viral RNA kit according to the manufactures (Cat. #R1035; Zymo Research). Luna Universal One-Step RT-qPCR kit was used to quantify viral genomic RNA (Cat. E3005S; New England Biolabs) with primer/probe sets for the SARS-CoV-2 E gene (Forward: 5'ACAGGTACGTTAATAGTTAATAGCGT Reverse: 5'-ATATTGCAGCAGTACGCACACA Probe: ACA CTAGCCATCCTTACTGCGCTTCG 5'Fam 3'QSY-1).<sup>35</sup> Standards were generated with known concentrations of viral RNA copies. A total of 5 µL of extracted RNA were run in duplicate on Applied Biosystems QuantStudio 3 (Thermo Fisher Scientific), and results were analyzed with Design and Analysis Software DA2 version 2.6.0.

### Histology

Left lobes of infected hamster lungs were isolated, fixed in 10% formalin for 1 wk at RT, and then transferred to 70% ethanol. Fixed tissues were processed and embedded in paraffin wax. The paraffin block was cut into 4 µm sections and placed on Superfrost Plus slides (Thermo Fisher Scientific). Sections were dried and duplicate sections were subjected to hematoxylin and eosin. Hematoxylin and eosin staining was done on a fully automated Leica ST5010-CV5030 system. Sections were imaged using a Zeiss AXIO Observer.A1 Inverted Fluorescence Microscope at 10X and 20X magnification.

Lung histology slides were evaluated using a standardized reporting criteria for pathologies induced by SARS-CoV-2 infections in hamsters.<sup>36</sup> Pathologies highly characteristic of SARS-CoV-2 induced pneumonia were assessed, including bronchial/peribronchial lesions, patchy throughout the lungs, diffuse alveolar damage, hyaline membranes, cellular debris in alveoli, intra-alveolar fibrin deposition, air spaces (restricted [+]; open [-]), hemorrhage, edema, vasculature damage/collapse, alveolar/interstitial pneumonia, intra-alveolar cells, perivascular lymphocytic cuffing, and hyperplasia of the bronchial epithelial cells (BECs)/alveolar epithelial cells (AECs). Lung histology slides demonstrating the assessed pathologies were assigned +1 each, contributing to the overall severity score.

### Neutralizing antibody titers

Serum and BAL samples from immunized groups were tested for neutralizing antibodies with a cPass SARS-CoV-2 Neutralizing Antibody Detection Kit (GenScript). The assay was performed according to the manufacturer's instructions. Samples were prepared in triplicate wells at 1:9 dilution and neat for serum and BAL samples, respectively. OD readings were acquired by a DTX 880 Plate Reader (Beckman Coulter) and percent inhibition values were calculated by the following formula. Bars represented mean percent inhibition ± SEM of triplicate wells.

$$\text{Percent Inhibition} = \left( 1 - \frac{\text{OD value of sample}}{\text{OD value of (-) Control}} \right) \times 100\%$$

### Graphs and statistical analysis

Results were analyzed and graphed using GraphPad Prism Software 10.2.0 (GraphPad Software). No data points were excluded from the study. Statistical assumptions of normality, homogeneity, and independence were met, before performing a parameter test. Furthermore, sample sizes were determined based on power calculations, suggesting 4 to 6 animals per immunization group.<sup>37</sup> For proliferation assays, antibody enzyme-linked immunosorbent assays (ELISAs), neutralizing antibody assays, and flow cytometric analysis, statistical differences were analyzed by 1- or 2-way analyses of variance, followed by adjustment for multiple comparisons. Spearman's test was performed to determine correlations between epitope-specific, protein-specific, and neutralizing antibody responses.  $P \leq 0.05$  was used to determine significance.

### Results

#### Epitope selection and characterization of LP<sub>Mix</sub> vaccine design

We selected 7 epitopes (P<sub>1-7</sub>) from the SARS-CoV-2 S, N, and M proteins, based on predictions of promiscuous binding

to multiple human major histocompatibility complex (MHC) class I/II molecules, presence of continuous and discontinuous B cell epitopes, CD4<sup>+</sup>/CD8<sup>+</sup> T cell epitopes, antigenic propensity, surface exposure, and epitope conservation across coronaviruses.<sup>16,18–28</sup> Selected epitopes were incorporated into a lipopeptide-based vaccine construct (Fig. 1A). LP<sub>1</sub>, derived from the receptor binding domain (RBD) of the S<sub>1</sub> subunit, is predicted to be a neutralizing antibody and CD8<sup>+</sup> T cell epitope.<sup>23,26,28</sup> It is conserved across SARS-CoV-2, MERS, SARS-CoV-1, HCoV-HKU1, HCoV-OC43, HCoV-NL43, and HCoV-229E,<sup>20,22,23,26</sup> and contains epitopes that could be presented by multiple human MHC class I and II molecules, HLA-DR, A1, and B1. LP<sub>2</sub> is an S<sub>2</sub>-derived B cell epitope, highly conserved across SARS-CoV-2 and SARS-CoV-1,<sup>20,22,28</sup> and could potentially induce viral fusion-inhibiting antibodies. LP<sub>3–5</sub> are N-derived epitopes that are predicted to be CD4<sup>+</sup>/CD8<sup>+</sup> T cell epitopes, conserved across beta-coronaviruses, and bind to multiple MHC class I (LP<sub>3</sub>: HLA.A3, A11, A68; LP<sub>4</sub>: HLA.A2, A3, A11, A68, B40; LP<sub>5</sub>: HLA.A2, A11, A31, A68) and MHC class II (LP<sub>3–5</sub>: HLA-DRB1.01) molecules.<sup>16,18–22</sup> LP<sub>6,7</sub> are M-derived epitopes and bind to multiple MHC class II (LP<sub>6</sub>: HLA-DRB1, DRB5, DPA1, DPB1; LP<sub>7</sub>: HLA-DRB1, DRB3, DRB5) molecules.<sup>19,22</sup>

Male C57BL/6 mice were intranasally immunized twice with LP<sub>Mix</sub> vaccine formulations at 2 different doses, at D0 and D14 (Fig. 1B). Seven days after the second immunization (D21), serum, BALs, spleens, and lungs were harvested to carry out multiple immunogenicity assays (Fig. 1C).

### Intranasal immunizations with LP<sub>Mix</sub> groups induced robust cross-variant reactive, systemic IgM, and mucosal IgA responses

First, serum IgM titers were tested against S epitopes, using peptide (P<sub>1</sub> or P<sub>2</sub>)-coated plates to establish epitope specificity. All LP<sub>Mix</sub> groups induced significantly higher S epitope-specific IgM titers, compared with the unimmunized group (Fig. 2A. I). P<sub>1</sub>-specific IgM titers were similar across the LP<sub>Mix</sub> groups, with LP<sub>Mix</sub>(10) inducing the highest titers, followed by LP<sub>Mix</sub>(10) + HKCC, LP<sub>Mix</sub>(1), and LP<sub>Mix</sub>(1) + HKCC (Fig. 2A. I). Similarly, LP<sub>Mix</sub>(10) induced significantly higher P<sub>2</sub>-specific IgM titers, compared with LP<sub>Mix</sub>(10) + HKCC, LP<sub>Mix</sub>(1), and LP<sub>Mix</sub>(1) + HKCC immunizations (Fig. 2A. I). P<sub>1</sub>- and P<sub>2</sub>-specific IgM titers displayed a dose-dependent response.

Next, to evaluate vaccine-induced systemic humoral responses and their capacity to cross-react with multiple SARS-CoV-2 variants, serum samples from LP<sub>Mix</sub>-vaccinated groups were tested against the Alpha (B.1.1.7), Beta (B.1.351), Delta (B.1.617), and Omicron (BA.1, BA.4/5, BQ1.1, EG.5) variants (Fig. 2A. II). Considering all variants together, serum samples from all LP<sub>Mix</sub> immunization groups induced significantly higher cross-variant IgM titers compared with the unimmunized group (Fig. 2A. II). LP<sub>Mix</sub>(10) and LP<sub>Mix</sub>(1) immunizations induced higher cross-variant IgM responses, compared with their respective adjuvant groups—with the exception of LP<sub>Mix</sub>(1) + HKCC showing higher IgM antibody titers against B.1.1.7 and B.1.351 (Fig. 2A. II). Considering all immunization groups, LP<sub>Mix</sub>(10) showed the highest cross-reactive IgM humoral response in blood (Fig. 2A. II).

Pearson's correlation showed P<sub>1</sub>-specific IgM titers significantly correlated with Alpha (B.1.1.7)-specific ( $r=0.52$ ),

Beta (B.1.351)-specific ( $r=0.64$ ), Delta (B.1.617)-specific ( $r=0.78$ ), Omicron (BA.1)-specific ( $r=0.76$ ), Omicron (BA.4)-specific ( $r=0.54$ ), and Omicron (BA.5)-specific ( $r=0.55$ ) IgM titers (Fig. 2A. III). Also, there were significant positive correlations between P<sub>2</sub>-specific IgM titers and Alpha (B.1.1.7)-specific ( $r=0.59$ ), Beta (B.1.351)-specific ( $r=0.72$ ), Delta (B.1.617)-specific ( $r=0.84$ ), and Omicron (BA.1)-specific ( $r=0.87$ ) IgM titers (Fig. 2A. III).

Next, mucosal IgA responses were examined in BAL of immunized mice against S-derived epitopes P<sub>1</sub> and P<sub>2</sub>. P<sub>1</sub>- and P<sub>2</sub>-specific IgA titers were highest for LP<sub>Mix</sub>(10) + HKCC and LP<sub>Mix</sub>(10) groups, followed by the LP<sub>Mix</sub>(1) + HKCC and LP<sub>Mix</sub>(1) groups (Fig. 2B. I). P<sub>1</sub>/P<sub>2</sub>-specific IgA titers showed a dose-dependent response, with HKCC adjuvant significantly increasing IgA titers (Fig. 2B. I).

Interestingly, LP<sub>Mix</sub>(10) and LP<sub>Mix</sub>(1) groups showed the highest cross-variant IgA response, across all variants tested (Fig. 2B. II), which was higher than the corresponding adjuvant groups, across all variants (Fig. 2B. II). In the mucosa, P<sub>1</sub>-specific IgA titers showed a significantly strong positive correlation with Delta (B.1.617)-specific ( $r=0.67$ ) IgA titers. P<sub>2</sub>-specific IgA titers demonstrated significantly strong correlations with Delta (B.1.617)-specific ( $r=0.58$ ), Omicron (BA.1)-specific ( $r=0.48$ ), and Omicron (BA.5)-specific ( $r=0.52$ ) IgA titers (Fig. 2B. III), whereas there were weak correlations of P<sub>1</sub>- and P<sub>2</sub>-specific IgA titers with other variants.

In conclusion, targeting S epitopes, P<sub>1</sub> and P<sub>2</sub>, by LP<sub>Mix</sub> immunizations induces a mucosal IgA and systemic IgM humoral response that cross-reacts with S antigens of multiple SARS-CoV-2 variants.

### LP<sub>1</sub> and LP<sub>2</sub> epitope sequence alignment and structural analysis

The presence of P<sub>1</sub>- and P<sub>2</sub>-specific antibodies have shown a strong positive correlation with the Alpha (B.1.1.7)-specific, Beta (B.1.351)-specific, Delta (B.1.617)-specific, and Omicron (BA.1, BA.4/5, BQ1.1, EG.5)-specific antibody titers (Fig. 2A, B). To understand this cross-reactivity, sequence alignment and 3-dimensional structural analysis of the 4 SARS-CoV-2 VOCs was performed. The LP<sub>1</sub> epitope had 1 misalignment in the Alpha/Beta (N501Y) and Delta (Y505Q) variants and 5 misalignments in the Omicron BA.1 (Q493R, G496S, Q498R, and Y505H) variant (Fig. 2C. I). However, the LP<sub>1</sub> epitope has similar 3-dimensional structure across the wild-type, Alpha, and Beta variants, short beta sheets (AA positions: 492–494), followed by a random coil loop (AA positions: 499–506) (Fig. 2C. I). Similarly, the Delta variant has a random coil loop extending AA positions 499 to 501, followed by a second beta sheet extending from AA positions 502 to 506 (Fig. 2C. I). The Omicron variant has an extended beta sheet from AA positions 492 to 497 and a random coil loop from AA positions 499 to 506 (Fig. 2C. I). Within the LP<sub>1</sub> epitope region, SARS-CoV-2 VOCs maintain a beta-sheet framework with a random coil loop structure, accentuating the structurally conserved nature of this epitope. The LP<sub>2</sub> epitope, on the other hand, is universally conserved sequentially and structurally across the Alpha, Beta, Delta, and Omicron variants, with an alpha helical structure (Fig. 2C. II). Immunoglobulins, present as B cell receptors and soluble antibodies, recognize foreign antigens based on structural characteristics and/or sequence similarity. Therefore, the cross-reactive antibody response induced by the LP<sub>Mix</sub> vaccine may be due to conserved sequence and

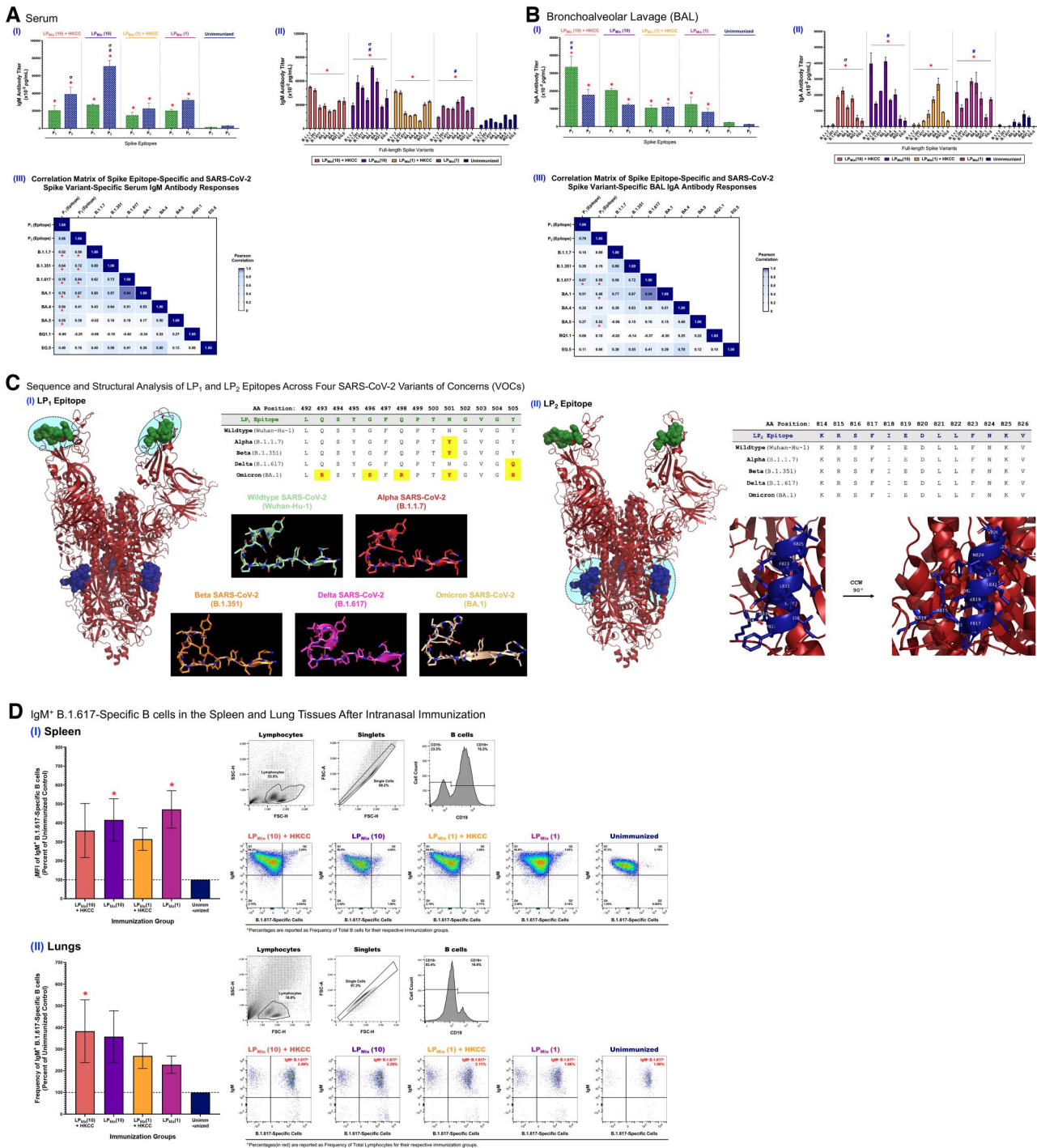


**Figure 2.** Intranasal immunizations with LP<sub>Mix</sub> groups, incorporating SARS-CoV-2 LP<sub>1</sub> and LP<sub>2</sub> S epitopes, led to cross-variant, S antigen-specific serum IgM and BAL IgA responses. Male C57BL/6 mice (n = 4–5/group) were immunized (D0, D14) intranasally with LP<sub>Mix</sub> immunization groups. Samples collected on D21 were assayed for (A. I) serum IgM and (B. I) BAL IgA titers against S epitopes (P<sub>1</sub> and P<sub>2</sub>), and S variant-specific (A. II) serum IgM and (B. II) BAL IgA antibodies, using ELISA. SARS-CoV-2 S proteins of the Alpha (B.1.1.7), Beta (B.1.351), Delta (B.1.617), and Omicron (BA.1, BA.4/5, BQ.1.1, EG.5) variants were tested. Pearson's correlation between S epitope-specific and SARS-CoV-2 S variant-specific antibody responses in the (A. III) serum (n = 15) and (B. III) BAL (n = 15) samples was conducted. Pearson's r values (black) and significant correlations (\*P ≤ 0.05) are indicated. (C) Sequence homology and 3-dimensional structural analysis of (I) LP<sub>1</sub> and (II) LP<sub>2</sub> epitopes across the wild-type (Wuhan-Hu-1; 6VW1), Alpha (B.1.1.7; 7EKF), Beta (B.1.351; 7WEV), Delta (B.1.617; 7W98), and Omicron (BA.1; 7T9K) variants of SARS-CoV-2. (D) Splenocytes and lung lymphocytes from LP<sub>Mix</sub> immunization groups were stimulated with PMA (50 ng/mL) and ionomycin (500 ng/mL). Using flow cytometry, integrated MFIs (MFIs) and frequencies of IgM<sup>+</sup> B.1.617-specific B cells (CD19<sup>+</sup> IgM<sup>+</sup> B.1.617<sup>+</sup>) were determined in the (I) spleen and (II) lung tissues. (A, B, D) Data are represented as mean ± SEM of triplicate wells/cultures from 3 independent repeat experiments. Two-way analysis of variance followed by Tukey's post hoc test was used to determine significance. \*, #, and σ indicate significant differences (P ≤ 0.05) between the immunized and unimmunized groups, the respective adjuvant and nonadjuvant groups, and the 10 μg versus 1 μg dose groups, respectively. CCW = counterclockwise.

structural features of the targeted epitopes in S antigens across the SARS-CoV-2 VOCs.

### Intranasal immunizations with LP<sub>Mix</sub> groups induced higher frequencies of IgM<sup>+</sup> S antigen-specific B cells in the spleen and lungs

The development of a robust vaccine-induced humoral response relies on the recruitment, activation, and maturation of antigen-specific B cells.<sup>38</sup> Therefore, we assessed the frequency and integrated MFIs (to reflect both the frequencies and MFI) of IgM<sup>+</sup> S-specific B cells in response to LP<sub>Mix</sub> immunizations.<sup>39</sup> IgM<sup>+</sup> S antigen (Delta, B.1.617)-specific B cell frequencies were higher in the spleen for all LP<sub>Mix</sub>-vaccinated groups compared with the unimmunized group (Fig. 2D, I, right). LP<sub>Mix</sub>(10) and LP<sub>Mix</sub>(1) immunization showed significant increases in surface expression of IgM and frequencies of IgM<sup>+</sup> Delta (B.1.617)-specific B cells (Fig. 2D, I, left) in the spleen. Notably, these results were consistent with cross-variant IgM responses induced by LP<sub>Mix</sub> immunization groups. In the lungs, IgM<sup>+</sup> Delta (B.1.617)-specific B cell frequencies for LP<sub>Mix</sub>(10) + HKCC, LP<sub>Mix</sub>(10), LP<sub>Mix</sub>(1) + HKCC, and LP<sub>Mix</sub>(1) groups were higher compared with those in the unimmunized group; however, only LP<sub>Mix</sub>(10) + HKCC was significant (Fig. 2D, II). Notably, lung IgM<sup>+</sup> Delta (B.1.617)-specific B cell frequencies increased in a dose-dependent fashion, with HKCC adjuvant further bolstering the response (Fig. 2D, II).

### Intranasal immunizations with LP<sub>Mix</sub> elicit a clinically effective neutralizing antibody response in blood and lungs

Neutralizing antibody responses have been suggested to correlate with protecting and preventing SARS-CoV-2 infections.<sup>14</sup> We assessed serum and BAL samples for their ability to block the S-ACE2 interaction, using a cPass SARS-CoV-2 surrogate viral neutralization kit. Serum antibody responses elicited by LP<sub>Mix</sub>(1) + HKCC and LP<sub>Mix</sub>(10) + HKCC immunizations showed the highest neutralizing capacity, with a percent inhibition of 36.5% and 34.0%, respectively (Fig. 3A). LP<sub>Mix</sub>(10) and LP<sub>Mix</sub>(1) immunizations showed 30.0% and 25.8% neutralizing capacity, respectively (Fig. 3A). All LP<sub>Mix</sub> immunizations had significantly higher neutralizing capacities compared with the unimmunized group (7.2%), and were well above the clinically significant threshold of 15% (Fig. 3A).<sup>40</sup> Interestingly, BALs also showed significant neutralizing capacity in response to LP<sub>Mix</sub>(10) + HKCC (37.6%), LP<sub>Mix</sub>(10) (32.1%), and LP<sub>Mix</sub>(1) + HKCC (28.8%) immunizations (Fig. 3A). Immunization with LP<sub>Mix</sub> alone at the lower concentration (1 µg) showed a percent inhibition of 18.8%, which was still significantly higher than the unimmunized group (5.6%), and above the clinically significant threshold (Fig. 3A). Overall, neutralizing antibody responses were higher for the 10-µg dose, and the addition of the HKCC adjuvant further increased the response in both the blood and lungs.

Furthermore, correlation studies between neutralizing antibody titers and S epitope-specific titers showed that P<sub>1</sub>-specific ( $r = 0.376$ ,  $P = 0.015$ ) and P<sub>2</sub>-specific ( $r = 0.288$ ,  $P = 0.039$ ) serum IgM titers moderately correlated with serum neutralizing antibody titers (Fig. 3B), whereas, P<sub>1</sub>-specific ( $r = 0.709$ ,  $P = 0.003$ ) and P<sub>2</sub>-specific ( $r = 0.701$ ,  $P = 0.004$ ) IgA titers strongly correlated with BAL neutralizing antibody titers (Fig. 3C). All in all, correlation studies reveal that humoral

responses against P<sub>1</sub> and P<sub>2</sub> S epitopes have strong neutralizing capacities, both systemically and mucosally.

### Intranasal immunizations with LP<sub>Mix</sub> elicit a robust N- and M-specific serum IgM and mucosal IgA antibody responses

Targeting the SARS-CoV-2 N and M proteins has shown to induce cross-reactive, long-lasting immune responses that protect against disease outcomes.<sup>41</sup> For all LP<sub>Mix</sub> immunizations, N- and M-specific serum IgM titers were significantly higher than the unimmunized group, and the addition of the HKCC adjuvant further bolstered titers (Fig. 4A). Also, we noted that N-specific IgM titers showed significant increases as the LP<sub>Mix</sub> dose increased (Fig. 4A). In the lungs, LP<sub>Mix</sub>(10) + HKCC and LP<sub>Mix</sub>(1) + HKCC immunizations induced significantly higher N-specific IgA titers compared with its respective nonadjuvant group and the unimmunized group (Fig. 4B). In contrast, overall, M-specific IgA titers were modest and not significant compared with the unimmunized group (Fig. 4B). Overall, humoral responses against the N and M proteins were more prevalent in the serum for all LP<sub>Mix</sub> immunization groups. However, in the lungs, only HKCC-adjuvanted groups induced a robust N- and M-specific antibody response.

### LP<sub>Mix</sub> immunizations generated a strong splenocyte proliferation response upon ex vivo stimulation with vaccine-targeted epitopes (P<sub>1-7</sub>)

The ability of antigen-specific lymphocytes to undergo clonal expansion is vital for the generation of a successful adaptive immune response.<sup>42</sup> Using BrdU proliferation assays, we assessed the recall responses of splenocytes derived from LP<sub>Mix</sub> immunizations against individual lipopeptides (LP<sub>1-7</sub>; solid bars) and peptides (P<sub>1-7</sub>; crosshatched bars) (Fig. 5). Considering all recall antigens, HKCC adjuvant groups generated significantly higher splenocyte proliferation responses compared with the no adjuvant groups (Fig. 5). Also, the 1-µg dose induced a significantly better proliferation responses compared with the 10-µg doses (Fig. 5). These results indicated that LP<sub>Mix</sub> immunizations induced antigen-specific lymphocytes in the spleen that can proliferate in response to recall antigens, highlighting the generation of antigen-specific adaptive responses.

### Intranasal immunizations with LP<sub>Mix</sub> elicited effector CTLs and Th T cells in spleen and lungs

Using flow cytometry, we examined the gross phenotype, distribution, and function of stimulated splenocytes derived from LP<sub>Mix</sub> immunizations. Phenograph identified 24 distinct CTL (CD3<sup>+</sup> CD4<sup>-</sup> CD8<sup>+</sup>) and Th cell (CD3<sup>+</sup> CD4<sup>+</sup> CD8<sup>-</sup>) clusters across the LP<sub>Mix</sub> immunization groups (Fig. 6A, B, D, and E). Next, cell clusters contributing to vaccine-induced effector responses (expressing any combination of CCR7, tumor necrosis factor α [TNFα], interferon γ [IFNγ], and/or interleukin [IL]-2) were identified, and cell counts (per 50,000 cells) were shown as vaccine responders (Fig. 6C and F). LP<sub>Mix</sub>(10) + HKCC showed the highest induction of effector CTLs, followed by LP<sub>Mix</sub>(10) and LP<sub>Mix</sub>(1) + HKCC (Fig. 6C). All of the immunized groups were higher than the control unimmunized group.

In the lungs, we identified 13 different CTL (CD3<sup>+</sup> CD4<sup>-</sup> CD8<sup>+</sup>) and 20 different Th cell (CD3<sup>+</sup> CD4<sup>+</sup> CD8<sup>-</sup>) clusters, distributed across LP<sub>Mix</sub> immunization groups (Fig. 7A, B, D,

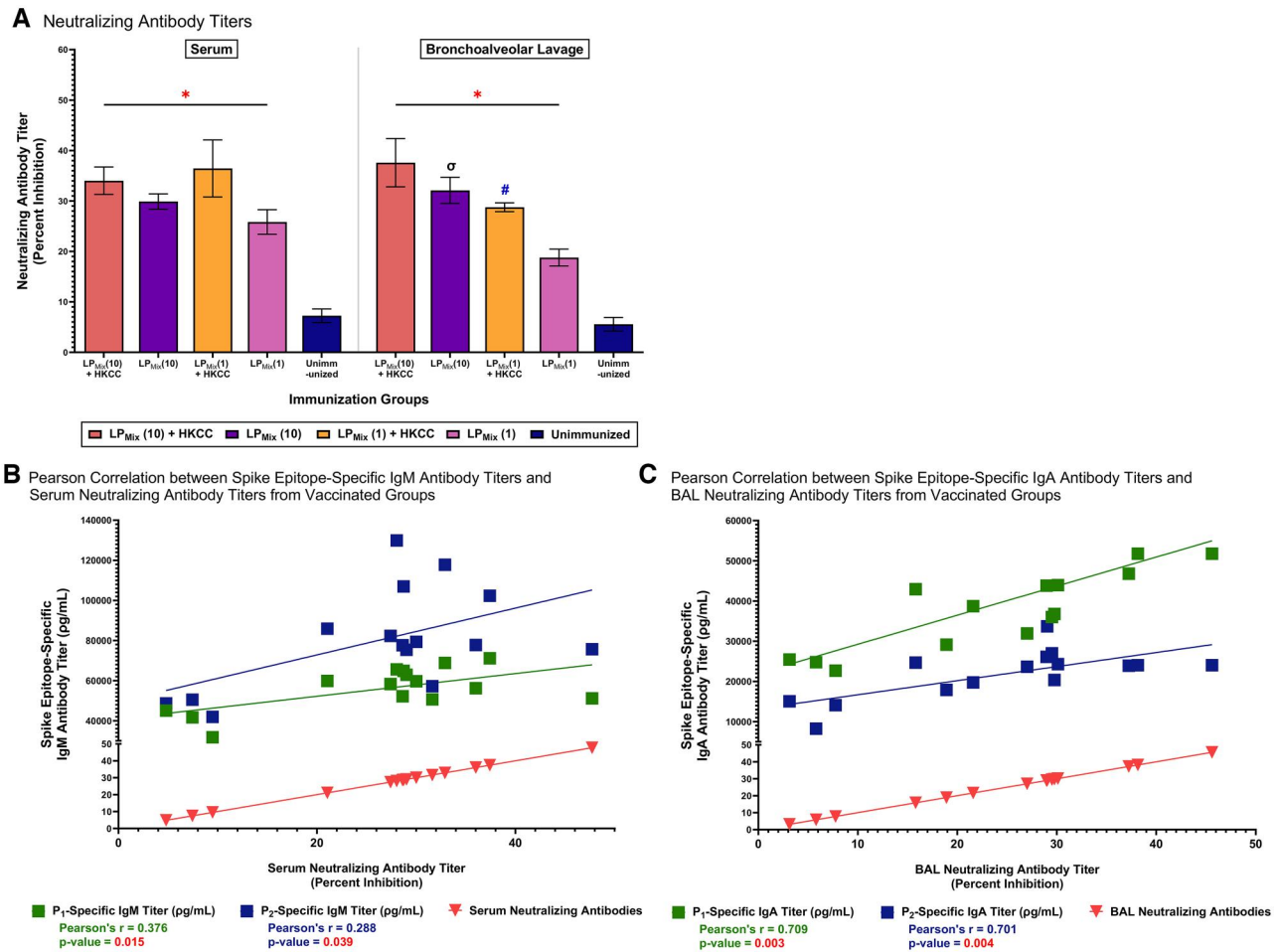


**Figure 3.** Intranasal immunizations with LP<sub>Mix</sub> groups, incorporating SARS-CoV-2 LP<sub>1</sub> and LP<sub>2</sub> S epitopes, induced strong neutralizing antibody titers in the serum and lung mucosa. (A) Male C57BL/6 mice ( $n = 4-5$ /group) were immunized intranasally with LP<sub>Mix</sub> groups, twice, 14 d apart. On D21, serum and BAL samples were collected to determine neutralizing antibody titers using a cPass surrogate viral neutralization assay. Serum (1:9) and BAL (1:1) samples were diluted and performed in triplicate wells. Data are mean  $\pm$  SEM and represent 3 independent repeat experiments. One-way analysis of variance followed by Sidák post hoc test was used to determine significance. \*, #, and  $\sigma$  indicate significant differences ( $P \leq 0.05$ ) between the immunized and unimmunized groups, the respective adjuvant and nonadjuvant groups, and the 10  $\mu$ g versus 1  $\mu$ g dose groups, respectively. Pearson's correlation between neutralizing antibody titers and P<sub>1</sub>/P<sub>2</sub>-specific antibody titers in the (B) serum ( $n = 15$ ) and (C) BAL ( $n = 15$ ) samples of mice, intranasally immunized with LP<sub>Mix</sub> groups.

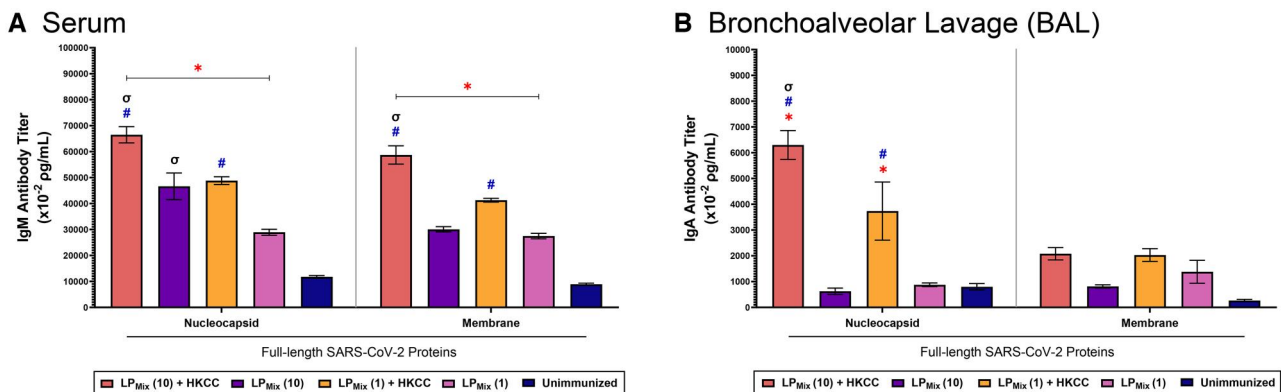


**Figure 4.** Intranasal immunizations with LP<sub>Mix</sub> groups induced a systemic IgM and mucosal IgA response against the SARS-CoV-2 N and M proteins. Male C57BL/6 mice ( $n = 4-5$ /group) were immunized (D0, D14) intranasally with LP<sub>Mix</sub> immunization groups. Serum samples and BALs were collected on D21, and assayed for IgM and IgA antibodies against the SARS-CoV-2 N and M proteins, using ELISA. Antibody concentrations were obtained by interpolating OD values using an appropriate standard curve. N- and M-specific (A) serum IgM and (B) BAL IgA antibody titers (pg/mL) were determined and presented as mean (Ig)  $\pm$  SEM of triplicate wells, from 3 independent repeat experiments. Two-way analysis of variance followed by Tukey's post hoc test was used to determine significance. \*, #, and  $\sigma$  indicate significant differences ( $P \leq 0.05$ ) between the immunized and unimmunized groups, the respective adjuvant and nonadjuvant groups, and the 10  $\mu$ g versus 1  $\mu$ g dose groups, respectively.

## Splenocyte Proliferation

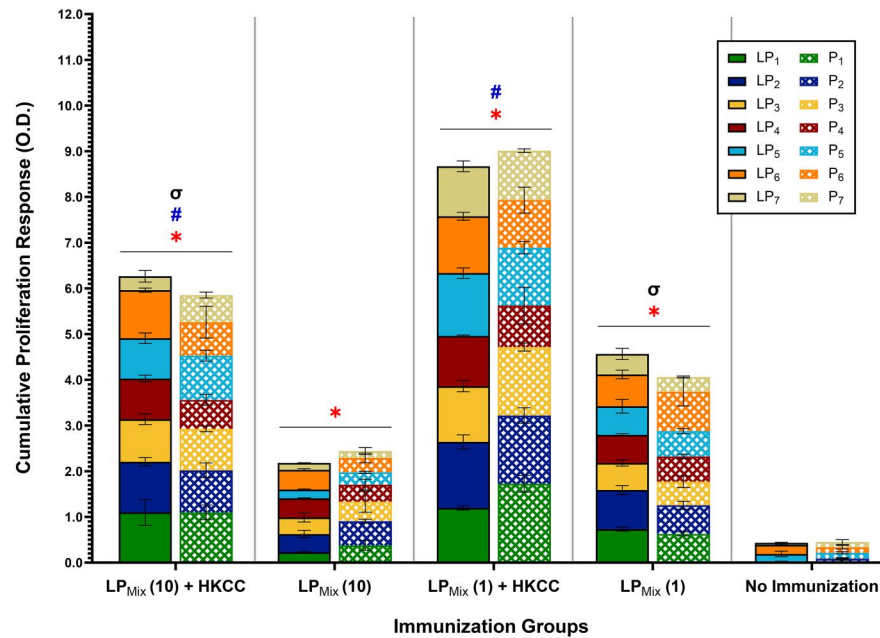


**Figure 5.** Intranasal immunizations with LP<sub>Mix</sub> groups induced antigen-specific splenocyte proliferation responses in mice. (A) Male C57BL/6 mice ( $n = 4-5/\text{group}$ ) were immunized intranasally on D0 and D14 with LP<sub>Mix</sub> immunization groups. On D21, splenocytes derived from immunized mice were cultured with irradiated antigen-presenting cells (from unimmunized syngeneic mice) and restimulated ex vivo with individual lipopeptides (LP<sub>1-7</sub>; solid bars) and peptides (P<sub>1-7</sub>; crosshatched bars), at 0.1  $\mu\text{g}/\text{mL}$  for 4 d. Proliferation was quantified by BrdU incorporation in proliferating cells. Unimmunized mice were used as control. Data are shown as mean  $\pm$  SEM of triplicate cultures and represent 3 independent repeat experiments. Statistical significance was determined by 2-analysis of variance, followed by Tukey's post hoc test. \*, #, and  $\sigma$  indicate significant differences ( $P \leq 0.05$ ) between the immunized and unimmunized groups, the respective adjuvant and nonadjuvant groups, and the 10  $\mu\text{g}$  versus 1  $\mu\text{g}$  dose groups, respectively.

and E). LP<sub>Mix</sub> immunizations resulted in higher frequencies of effector vaccine responder CTLs, defined by expression of any combination of CCR7, TNF $\alpha$ , IFN $\gamma$ , and/or IL-2, compared with unimmunized (Fig. 7C). Among the immunized groups, LP<sub>Mix</sub>(10) + HKCC, LP<sub>Mix</sub>(10), and LP<sub>Mix</sub>(1) + HKCC immunizations exhibit higher numbers of effector vaccine responder cells compared with the LP<sub>Mix</sub>(1) group. Interestingly, at lower dose of LP<sub>Mix</sub>(1), HKCC adjuvant demonstrated a higher bolstering of the response than at the higher dose. Effector vaccine responder Th cells also demonstrated a higher number in the immunized groups compared with those unimmunized (Fig. 7F).

#### Efficacy of LP<sub>Mix</sub> vaccine in a SARS-CoV-2 hamster infection model

To evaluate the ability of our vaccine to mediate protection against SARS-CoV-2 infections, we identified the most immunogenic LP<sub>Mix</sub> formulations, LP<sub>Mix</sub>(10) and LP<sub>Mix</sub>(10) + HKCC, to test in a SARS-CoV-2 infection model. Hamsters ( $n = 5-6/\text{group}$ ) were immunized twice, 14 d apart (D24, D10), and intranasally challenged (D0) with the SARS-CoV-2 BA.5 variant (Fig. 8A). Hamsters, an outbred animal model of SARS-CoV-2 infection, do not show clinical symptoms of the COVID disease. The only clinical parameter used is weight loss upon infection. Over the course of 5 d postinfection, groups of hamsters experienced a median weight loss of 6.4% to 9.4%; however, 1 hamster was an outlier in the unimmunized group and did not show weight loss as shown in Fig. 8B. Due to the variation in weight loss, no statistical significance was observed between the immunized and unimmunized groups (Fig. 8B). Serum samples were collected prior

to infection on D0 and assayed for neutralizing antibodies. LP<sub>Mix</sub>(10) and LP<sub>Mix</sub>(10) + HKCC immunizations induced significantly higher neutralizing antibody titers, with a percent inhibition of 24.0% and 22.5%, respectively, compared with the unimmunized animals at  $\sim 17\%$  (Fig. 8C).

Next, we measured the genomic or single-guide RNA (sgRNA) to determine viral loads in oral swabs, nasal washes, and lung tissues to assess the effectiveness of our vaccine to clear and to protect against SARS-CoV-2 infections. In oral swabs, unimmunized hamsters exhibited a natural ability to reduce viral burden from D3 to D5 postinfection. Notably, LP<sub>Mix</sub>(10) immunizations led to a reduction in viral burden by 61.9% and 55.2% on D3 and D5 postinfection, respectively, compared with their corresponding unimmunized group (Fig. 8D). LP<sub>Mix</sub>(10) + HKCC immunizations did not reduce viral RNA burdens on D3 postinfection; however, by D5 the viral RNA was reduced by 66.2% compared with the corresponding unimmunized group (Fig. 8D). Nasal washes collected 3 d after infection revealed that LP<sub>Mix</sub>(10) immunizations reduced viral loads by  $\sim 90\%$  compared with the LP<sub>Mix</sub>(10) + HKCC and unimmunized groups (Fig. 8E). Similarly, the viral RNA burden in the lungs of LP<sub>Mix</sub>(10)-immunized hamsters was reduced by 53.3% compared with the unimmunized group (Fig. 8F). Interestingly, the LP<sub>Mix</sub>(10) + HKCC group demonstrated a higher viral sgRNA compared with unimmunized group. Notably, within the unimmunized group, 1 hamster with no weight loss still had high viral loads/burdens in oral swabs, nasal washes, and lung tissue (Fig. 8B, D-F).

Most importantly, we examined lung histology to evaluate the ability of our vaccine formulations to minimize

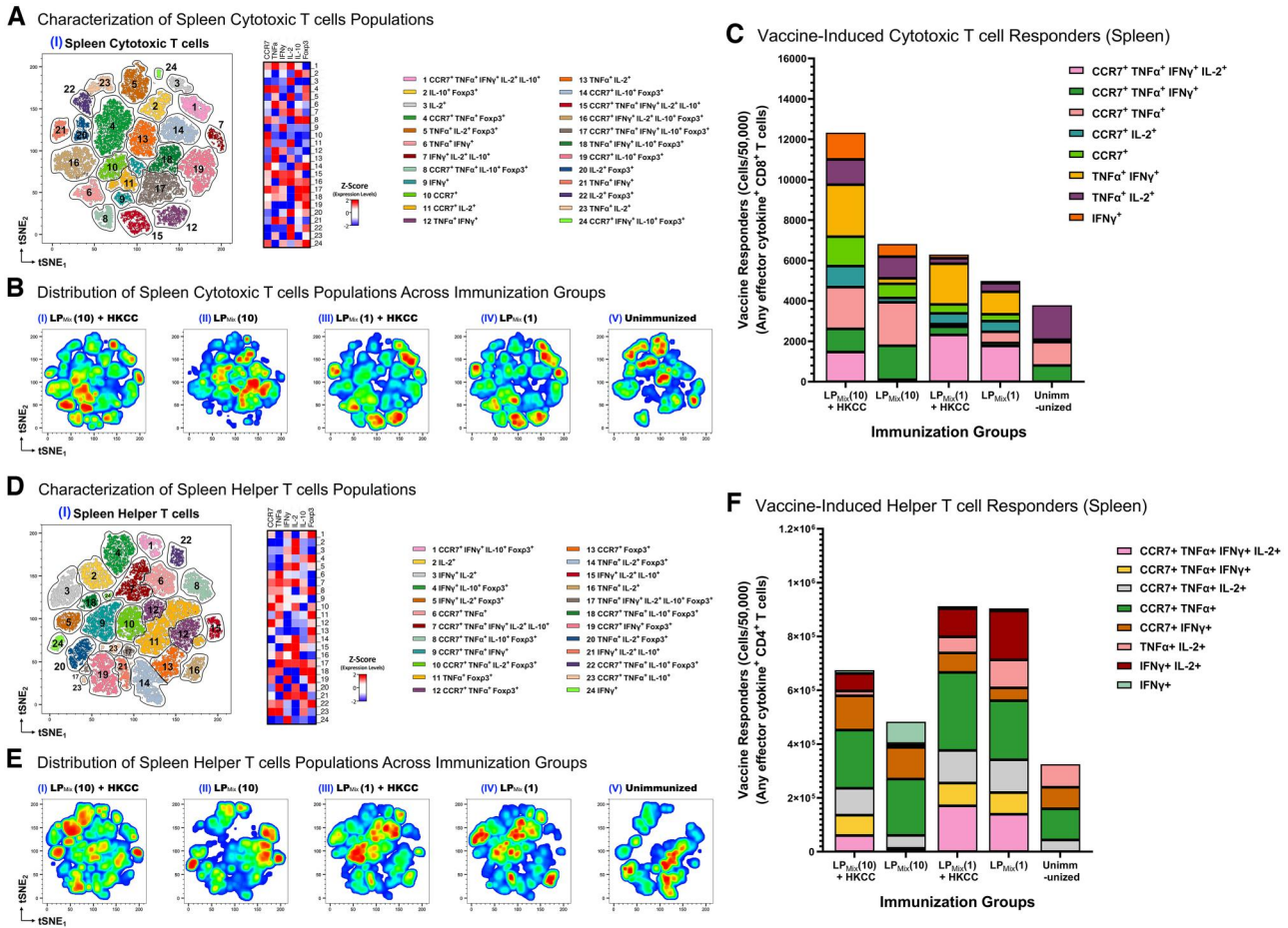


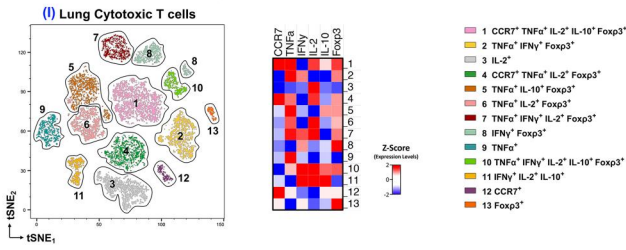
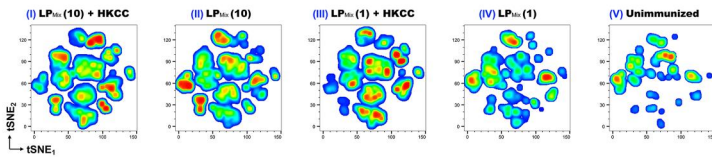
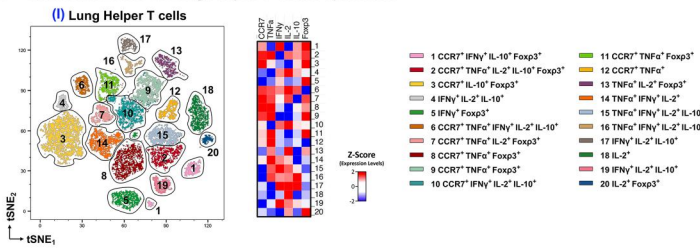
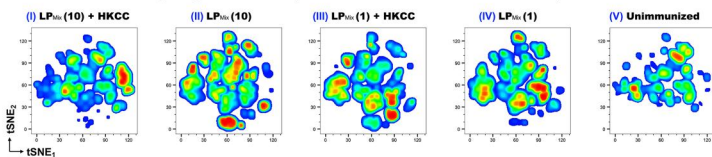
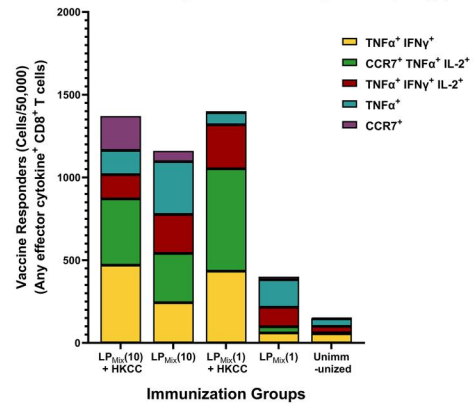
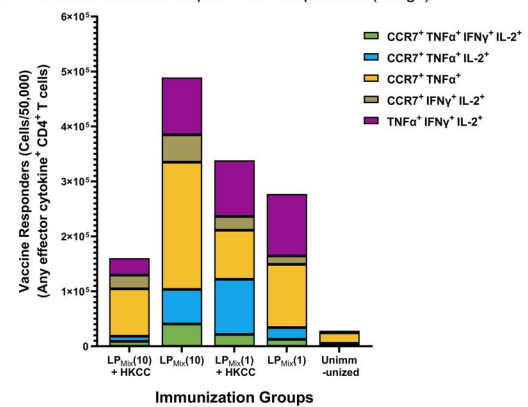
**Figure 6.** Phenotypic analysis of splenic cytotoxic and Th cells in mice immunized with LP<sub>Mix</sub> groups. (A) Cytotoxic and (D) Th cell clusters were identified by t-distributed stochastic neighbor embedding (t-SNE) plots from concatenated spleen samples of LP<sub>Mix</sub> immunized mice (each LP<sub>Mix</sub> group: n = 3; unimmunized: n = 3; total: n = 15). Each identified cytotoxic and Th cell cluster was indicated by color and number (1–24). Heatmaps showed the expression profiles of each cluster, for the cytotoxic and helper T cell populations. Pseudocolor density plots showed the distribution of splenic (B) cytotoxic and (E) Th cell populations across the LP<sub>Mix</sub> immunization groups: (I) LP<sub>Mix</sub>(10) + HKCC, (II) LP<sub>Mix</sub>(10), (III) LP<sub>Mix</sub>(1) + HKCC, (IV) LP<sub>Mix</sub>(1), and (V) unimmunized. Red represents clusters in high-density areas and blue represents low-density areas. Cell counts of vaccine-induced (C) cytotoxic and (F) Th cells expressing any combination of CCR7, TNF $\alpha$ , IFN $\gamma$ , and/or IL-2, stratified by vaccine group: LP<sub>Mix</sub>(10) + HKCC, LP<sub>Mix</sub>(10), LP<sub>Mix</sub>(1) + HKCC, LP<sub>Mix</sub>(1), and unimmunized. Bar graphs are representative of 3 independent repeats, flow cytometry experiments.

pathologies resulting from SARS-CoV-2 infections. Hamsters immunized with LP<sub>Mix</sub>(10) and LP<sub>Mix</sub>(10) + HKCC showed significantly lower severity scores compared with the unimmunized group (Fig. 8G). Lungs from unimmunized hamsters exhibited significant alveolar infiltration of red blood cells, cellular debris, and other resident cells, along with thickening of the alveolar septum, hyperplasia of the alveolar and bronchial epithelial cells, extensive hemorrhaging, and the presence of hyaline membranes, indicative of diffuse alveolar damage (Fig. 8H, I–III). Notably, we observed milder pathologies with LP<sub>Mix</sub>(10)- and LP<sub>Mix</sub>(10) + HKCC-immunized lungs, characterized by substantially less alveolar infiltrate, little to no hemorrhaging, absence of hyaline membranes, and the presence of unobstructive airspaces to facilitate efficient oxygen exchange (Fig. 8H, IV–IX).

**Discussion**

During the pandemic, several highly efficacious vaccines were developed and implemented. However, emerging SARS-CoV-

2 variants have challenged vaccine efficacies and diminished vaccine-induced immunity. Therefore, there is a need for a next-generation vaccine that broadly protects and prevents infections against SARS-CoV-2, its variants, and related coronaviruses. Due to similarities in various antigens between SARS-CoV-2, MERS, and other common cold coronaviruses, many preclinical/clinical vaccine studies have reported vaccine-induced cross-reactive antibody titers.<sup>43–47</sup> To induce variant-specific immunity, current approaches are focusing on periodically updating vaccine composition and administering repeated booster shots. However, these may result in immune imprinting and antigenic sin phenomena, leading to a compromised vaccine efficacy. Pre-existing antibodies specific for the Wuhan-Hu-1 strain have been shown to be imprinted and increased with each homologous boosting with BNT162b2 mRNA vaccine, and heterologous boosting with bivalent vaccines that incorporate S proteins of novel SARS-CoV-2 VOCs.<sup>44,47,48</sup> Vaccine-induced imprinting results in back-boosting of original humoral immunity while limiting the generation of de novo antibodies against novel

**A** Characterization of Lung Cytotoxic T cells Populations**B** Distribution of Lung Cytotoxic T cells Populations Across Immunization Groups**D** Characterization of Lung Helper T cells Populations**E** Distribution of Lung Helper T cells Populations Across Immunization Groups**C** Vaccine-Induced Cytotoxic T cell Responders (Lungs)**F** Vaccine-Induced Helper T cell Responders (Lungs)

**Figure 7.** Phenotypic analysis of lung cytotoxic and Th cells in mice immunized with LP<sub>Mix</sub> groups. (A) Cytotoxic and (D) Th cell clusters were identified by t-distributed stochastic neighbor embedding (t-SNE) plots from concatenated lung samples of LP<sub>Mix</sub>-immunized mice (each LP<sub>Mix</sub> group: n = 3; unimmunized: n = 3; total: n = 15). Each identified cytotoxic and helper T cell cluster was indicated by color and number (1–13 and 1–20, respectively). Heatmaps showed the expression profiles of each cluster for the cytotoxic and Th cell populations. Pseudocolor density plots showed the distribution of lung (B) cytotoxic and (E) Th cell populations across the LP<sub>Mix</sub> immunization groups: (I) LP<sub>Mix</sub>(10) + HKCC, (II) LP<sub>Mix</sub>(10), (III) LP<sub>Mix</sub>(1) + HKCC, (IV) LP<sub>Mix</sub>(1), and (V) unimmunized. Red represents clusters in high-density areas and blue represents low-density areas. Cell counts of vaccine-induced (C) cytotoxic and (F) Th cells expressing any combination of CCR7, TNFα, IFNγ, and/or IL-2, stratified by vaccine group: LP<sub>Mix</sub>(10) + HKCC, LP<sub>Mix</sub>(10), LP<sub>Mix</sub>(1) + HKCC, LP<sub>Mix</sub>(1), and unimmunized. Bar graphs are representative of 3 independent repeat flow cytometry experiments.

SARS-CoV-2 VOCs and conserved epitopes.<sup>45</sup> Therefore, next-generation vaccines need to establish cross-reactive antibodies by targeting conserved broadly protective epitopes that are resistant to variant-specific changes, while avoiding pooling S proteins from different SARS-CoV-2 VOCs to establish cross-reactivity. In our study, interestingly, LP<sub>Mix</sub> immunizations elicited cross-reactive IgM/IgA titers against 9 different SARS-CoV-2 S variants. LP<sub>Mix</sub> induced its component P<sub>1</sub>/P<sub>2</sub>-specific antibodies that are structurally and/or sequentially conserved epitopes from the Wuhan to Omicron VOCs and strongly correlate with multiple SARS-CoV-2 VOCs IgM/IgA titers. The addition of adjuvant HKCC (with the 10 μg LP<sub>Mix</sub> dose) quantitatively enhanced the IgA binding to both P<sub>1</sub> and P<sub>2</sub> in ELISA (Fig. 2B. I), supporting its role as a mucosal adjuvant in enhancing overall IgA response to the targeted epitopes. However, the binding to variant S antigen did not show the same pattern. It is possible that the adjuvant redirected IgA responses to epitopes/configuration in variant S antigens not exposed in ELISA plates. Furthermore, administering full-length S proteins may focus immune responses toward immunodominant, hypervariable regions that promotes imprinting, whereas epitope-based vaccines

can direct responses toward conserved, cryptic domains, such as S<sub>2</sub> (targeted by LP<sub>2</sub>) as well, thereby establishing cross-reactivity while limiting antigenic sin. These findings suggest that next-generation vaccines that target conserved regions of S provide more effective and sustainable cross-reactive titers and may limit antigenic sin.

nAb titers strongly correlate with protection against SARS-CoV-2 infections, and vaccine efficacy. Our study demonstrated all LP<sub>Mix</sub> vaccines induced strong serum nAb titers, with HKCC upregulating nAbs in the mouse model (Fig. 4). Importantly, for viral infections, establishing titers of nAbs in the lung mucosa can block viral entry at the site of infection. Examining BAL samples, we found LP<sub>Mix</sub> vaccines with increased dose, and the addition of HKCC induced higher nAbs titers (Fig. 4). LP<sub>Mix</sub>-induced nAbs titers are expected to be comprised of P<sub>1</sub> (S<sub>1</sub>-RBD-epitope) and P<sub>2</sub> (S<sub>2</sub>-epitope) antibodies. Mechanistically, they can contribute to neutralization by blocking the S-ACE2 interaction, and interfering with viral fusion processes and/or antibody-dependent allosteric hindrance of the S-ACE2 interaction, respectively.<sup>29</sup> Because next-generation vaccines aim to protect against a broad spectrum of coronaviruses, screening for conserved,

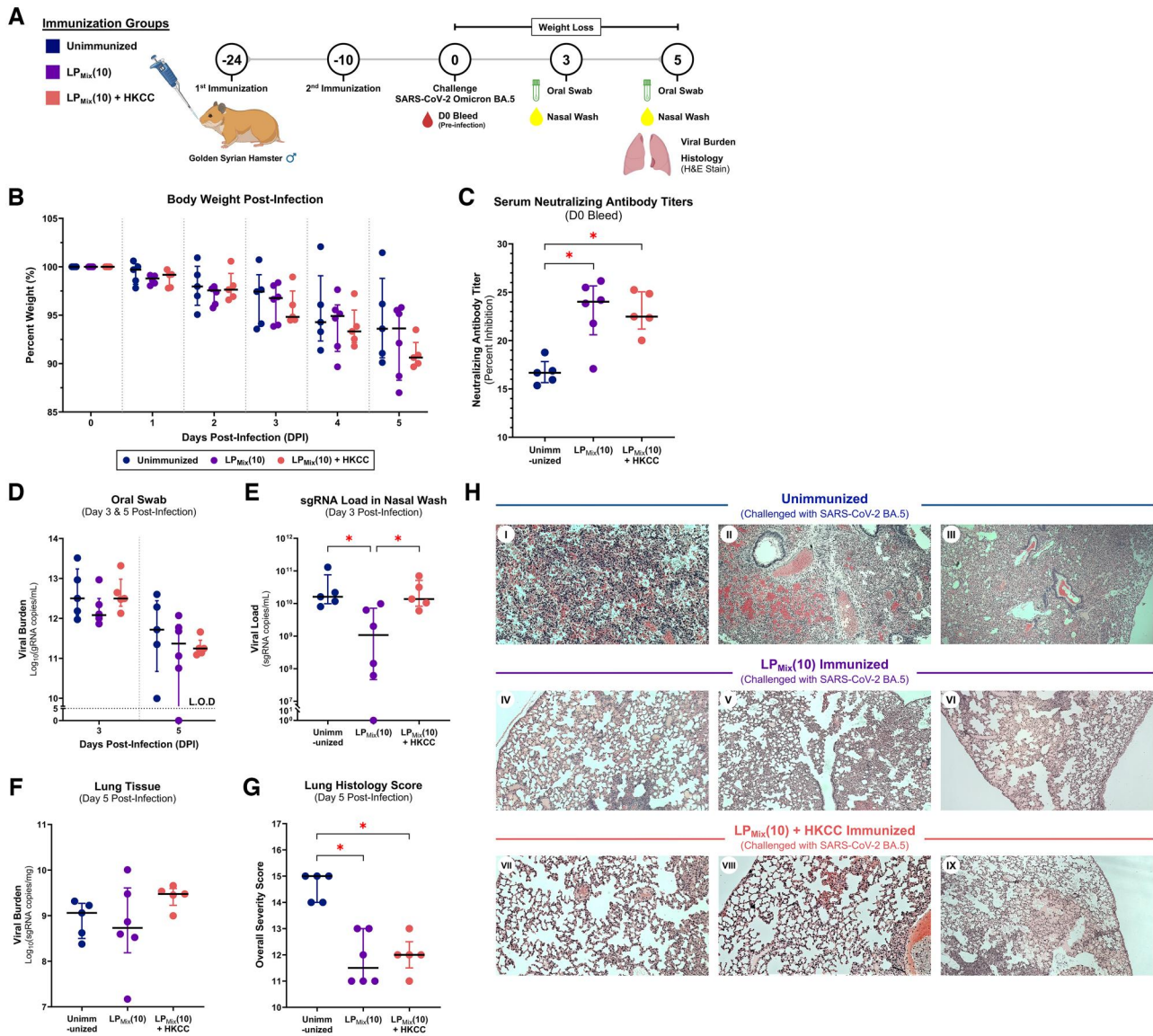


**Figure 8.** Vaccine efficacy of LP<sub>Mix</sub> vaccine in hamsters challenged with the SARS-CoV-2 Omicron BA.5 variant. (A) Immunization and sample collection regimen: Syrian hamsters were immunized (D24, D10) with LP<sub>Mix</sub>(10) (n = 6) and LP<sub>Mix</sub>(10) + HKCC (n = 5), and the control group was unimmunized (n = 5). Ten days after the second immunization, hamsters were intranasally challenged with a 50% tissue culture infectious dose of  $1.67 \times 10^5$  of the SARS-CoV-2 Omicron BA.5 variant. (B) Weight loss was monitored for 5 d postinfection (n = 5–6/group). (C) D0 (preinfection) serum samples were assayed for neutralizing antibody titers using a cPass surrogate viral neutralization assay. (D) Detection of SARS-CoV-2 gRNA copies in oral swabs on D3 and D5 postinfection were quantified. SARS-CoV-2 sgRNA copies in the (E) nasal washes (D3, D5) and (F) lung tissues (D5) were quantified. (G) Histopathological analysis of hematoxylin and eosin (H&E)-stained lung sections, collected on D5 postinfection, were scored from 0 (no severity) to 15 (most severity) based on a standardized evaluation criteria for lung pathologies in SARS-CoV-2-infected hamsters.<sup>36</sup> (H) Representative hematoxylin and eosin-stained sections are shown from immunized lungs of (I–III) unimmunized, (IV–VI) LP<sub>Mix</sub>(10), and (VII–IX) LP<sub>Mix</sub>(10) + HKCC groups. (C–G) Data are shown as median  $\pm$  interquartile range (IQR), with data points shown for individual hamsters. Statistical significance (\*P  $\leq$  0.05) was determined by Kruskal-Wallis test, followed by Dunn's multiple comparisons test.

functionally blockable S epitopes, that go beyond RBD, is a promising avenue for achieving broad protection. Our studies confirm that P<sub>1</sub>/P<sub>2</sub>-specific antibodies induced by LP<sub>Mix</sub> immunizations correlate with cross-reactivity among 9 SARS-CoV-2 variants and with neutralizing function. Another important consideration is that neutralization and clearance of virus infection require more than targeting S antigen. A recent study revealed that SARS-CoV-2-infected cells secrete the N protein, which can neutralize 11 human chemokines, hampering the recruitment and communication between immune cells.<sup>49</sup> Therefore, N-specific antibodies may play a vital role in neutralizing viral shedding of the N protein and restoring

chemokine functionality during a SARS-CoV-2 infection. This possibly explains strong correlates between N-specific antibodies and protection against disease severity.<sup>21,27</sup> In addition, the presence of M-specific antibody is indicative of a robust T cell response against the M protein.<sup>19,21,27</sup> Importantly, antibodies can facilitate numerous effector functions besides viral neutralization, including antibody-dependent cellular cytotoxicity, complement activation, complement dependent cellular cytotoxicity, phagocytosis, and opsonization. In this study, all LP<sub>Mix</sub> immunizations induced serum N/M-specific antibody titers, whereas in BAL samples, only LP<sub>Mix</sub> + HKCC vaccine formulations bolstered N/M-

specific antibodies. Taken together, LP<sub>Mix</sub> targets the SARS-CoV-2 S, N, and M proteins, leading to a multidimensional and multifunctional humoral response against SARS-CoV-2.

Next, cellular immunity plays a vital role in recognizing, controlling, and eliminating SARS-CoV-2 infections. Two parallel studies by Bergamaschi et al.<sup>51</sup> and Notarbartolo et al.<sup>50</sup> demonstrated that the early development of CD8<sup>+</sup> T cell responses, within 7 d of infection, correlated with effective viral clearance and mild disease outcomes. In our study, LP<sub>Mix</sub> immunizations induced higher proportions of effector CD8<sup>+</sup> T cells in the spleen of mice 7 d after the second immunization. Notably, only LP<sub>Mix</sub>(10) and LP<sub>Mix</sub>(10) + HKCC immunizations induced higher proportions of effector CD8<sup>+</sup> T cells in the lungs of mice, and upon viral challenge of hamsters with BA.5, effectively reducing lung pathologies. Taken together, LP<sub>Mix</sub> immunizations generated a CD8<sup>+</sup> T cell response that can contribute to protecting against disease outcomes and demonstrated measurable efficacy against the BA.5 variant.

During COVID infections, the functional capacity of immune cells is a major determinant in improving clinical outcomes and also establishing long-term immunity. In asymptomatic cases, T cell profiles showed coexpression of IFN $\gamma$ /TNF $\alpha$  and IL-10/Foxp3, whereas symptomatic cases showed more polarized T cell phenotypes that expressed inflammatory cytokines.<sup>17</sup> Within the effector CD8<sup>+</sup> T cell population, 4 of 5 and 5 of 12 cell clusters mimicked T cell profiles observed in asymptomatic cases, in lungs and spleen, respectively. Next, CD4<sup>+</sup> T cells expressing IFN $\gamma$ , TNF $\alpha$ , and IL-2 demonstrated the ability to stimulate B cells to undergo isotype switching and affinity maturation, facilitating the generation of de novo antibodies, with improved effector function, higher affinity, and tissue specificity.<sup>52</sup> Additionally, these T cell populations can enhance CD8<sup>+</sup> T cell cytotoxicity and promote the generation of memory cells.<sup>53</sup> Next, CD4<sup>+</sup> T cells expressing IFN $\gamma$ , TNF $\alpha$ , and IL-2 demonstrated the ability to stimulate B cells to undergo isotype switching and affinity maturation, facilitating the generation of de novo antibodies, with improved effector function, higher affinity, and tissue specificity.<sup>52</sup> Additionally, these T cell populations can enhance CD8<sup>+</sup> T cell cytotoxicity and promote the generation of memory cells.<sup>53</sup> LP<sub>Mix</sub> immunizations exhibited similar effector CD4<sup>+</sup> T cell functionality, defined by higher expression of CCR7, IFN $\gamma$ , TNF $\alpha$ , and IL-2 in the lungs and spleen, indicative of a well-orchestrated immune response that enhances cytotoxic function of CD8<sup>+</sup> T cells, promotes T cell-dependent B cell help, and facilitates the transition from effector-to-memory responses (Figs. 6 and 7). Ultimately, these responses together contribute to controlling viral replication, reducing viral loads, mitigating against severe disease outcomes, and improving vaccine efficacy.<sup>54–57</sup>

To achieve high vaccine efficacy, the induction of adaptive immunity and its inherent specificity is crucial for generating an optimal protective response. In our study, LP<sub>Mix</sub> immunizations induced splenocyte proliferation responses against S (P<sub>1</sub>/P<sub>2</sub>), N (P<sub>3</sub>/P<sub>4</sub>/P<sub>5</sub>), and M (P<sub>6</sub>/P<sub>7</sub>) antigens, providing insights into antigen recall responses and clonal expansion of antigen-specific lymphocytes (Fig. 5). In the gross splenocytes proliferation assay, both T and B cells clonally expand, which promotes heterogeneity within expanded populations, highlighted by the number of unique clusters identified in CTL and Th populations in the spleen by flow cytometry (Figs. 6 and 7). Furthermore, LP<sub>Mix</sub> immunizations induced

adaptive immunity (including cellular and humoral) and its specificity against each SARS-CoV-2 structural protein, which can work in different capacities to clear infections and protect against disease outcomes. Many studies have shown that S-specific T cells are more resistant to variant-specific changes, as only 3% and 7% of CD4<sup>+</sup> and CD8<sup>+</sup> T cell epitopes were affected by mutations acquired by SARS-CoV-2 VOCs, respectively.<sup>15,16,19,24</sup> This provides better immune control over viral replication and makes it more difficult for antigenic viral variants to escape. Beyond S, N/M-specific T cell responses have been correlated with protection against severe disease outcomes, T cell cross-reactivity, and the induction of long-term memory responses against coronaviruses.<sup>15–17,21</sup> Le Bert et al.<sup>58</sup> showed that N-specific T cells induced by SARS-CoV-1 infections were cross-reactive against the SARS-CoV-2 N protein, displaying immunity established 17 yr earlier. Also, the induction of M-specific cellular responses further broadens the coverage of coronaviruses as the M protein is evolutionary conserved across betacoronaviruses. As such, LP<sub>Mix</sub> immunizations with HKCC elicited higher N/M-specific cellular responses, suggesting a broadly protective, long-lasting response. These data support the development of HKCC as a functional mucosal adjuvant.

Ultimately, the innate and adaptive responses work to establish vaccine efficacy against infectious disease. We tested our LP<sub>Mix</sub> vaccine candidates in a Syrian hamster infection model that recapitulates several aspects of severe COVID-19. In this model, higher nAb titers protected against SARS-CoV-2 infections and lower viral loads.<sup>59</sup> Interestingly, both LP<sub>Mix</sub> vaccines induced similar levels of serum nAbs, however only LP<sub>Mix</sub>(10)-immunized hamsters showed a lower viral sgRNA in the upper and lower respiratory tract (Fig. 8E and F). The SARS-CoV-2 virion can be transmitted efficiently between individuals via direct contact or by aerosols; therefore, reduction in viral loads reflects the vaccines' ability to reduce viral transmissibility. It is possible that the dose of HKCC adjuvant used in these experiments, which was directly taken from mouse experiments, needs to be optimized in hamster model. It has been shown that sgRNA has a far longer stability than the viral antigen detection and culture positivity.<sup>60</sup> Therefore, although a reduction in sgRNA level represents reduction in infectious virus load, no reduction in sgRNA level may not necessarily represent infectious virus levels. In addition, increased phagocytosis and persistence of sgRNA in immune cells or in immune complexes may also allow longer detection of viral sgRNA.<sup>61</sup>

The hamster model accurately replicates severe COVID-19 conditions, characterized by lung pathologies, including diffuse alveolar damage, hyaline membranes, edema, cellular infiltration, and pneumonia. Unimmunized hamsters demonstrated these pathologies, whereas both LP<sub>Mix</sub>(10)- and LP<sub>Mix</sub>(10) + HKCC-immunized hamsters showed no hyaline membranes, no hemorrhages, and overall fewer lung pathologies (Fig. 8G and H). Brocato et al.<sup>62</sup> demonstrated that the absence of functional B and T cells led to hemorrhages and severe edema in Syrian hamsters infected with SARS-CoV-2, lending support that LP<sub>Mix</sub> immunizations effectively induced adaptive humoral and cellular responses. These results suggest both LP<sub>Mix</sub> vaccines mediated protection against severe COVID-19 disease outcomes.

Looking to the future, next-generation vaccines must be investigated in the context of preparing for the next pandemic. Inevitably, coevolution of host-virus immunity predicts

vaccine-induced and/or naturally acquired immunity will wane, and therefore, protection will diminish. However, maintaining a housekeeping level of protection against SARS-CoV-2 and other heterologous coronaviruses can prevent hospitalization and mortalities during a pandemic, until a VOC-specific vaccine is implemented. With housekeeping CoV vaccines, the focus would be to target broadly protective, conserved epitopes to maintain a basal yet sufficient coverage of circulating coronaviruses over time. In future studies, we will be looking at long-term sustained memory responses and immunity against endemic and emerging coronaviruses. Epitope-based vaccines have better safety profiles but often require an adjuvant. Another subunit peptide-based vaccine, CoVac-1, comprising peptides derived from SARS-CoV-2 S, N, M, and ORF-8 antigens, supplemented with Toll-like receptor 1/2 agonist XS15 emulsified in Montanide ISA51 as adjuvant, induced strong T cell immunity, comparable to our LP<sub>Mix</sub>, and is undergoing clinical testing.<sup>63</sup> However, CoVac-1 does not induce humoral immunity, in contrast to our LP<sub>Mix</sub> vaccine. The LP<sub>Mix</sub> vaccine induced both humoral and cellular responses without any adjuvant assistance because of the palmitoyl attachment, which enables micelle formation and self-adjuvanting properties.<sup>29</sup> Nevertheless, the addition of HKCC adjuvant further enhanced nAb titers, N-specific antibody titers, and antigen-specific proliferation responses. Most importantly, LP<sub>Mix</sub> vaccine demonstrated the induction of both mucosal and systemic multispecific immunity upon mucosal administration. In conclusion, our studies with LP<sub>Mix</sub> support its development as a next-generation vaccine for SARS-CoV-2 VOCs and related coronaviruses.

## Acknowledgments

The authors thank Jie Li for excellent technical assistance and Aja Rieger from flow cytometry core of the Faculty of Medicine and Dentistry, University of Alberta for support. The authors thank the NRC Animal Resources Group for their support in animal husbandry and Shawn Makinen, Luc Lemay, and Jennifer Wellman for their animal technical support within the CL-3 facility.

## Author contributions

Conceptualization, B.A., R.S.P., R.K.; methodology, R.S.P., D.D., J.B., M.H., J.K.S., R.K., A.T., B.A.; data analysis, B.A. and R.S.P.; writing—original draft preparation, B.A. and R.S.P.; writing—reviewing and editing, B.A., R.S.P.; supervision, B.A.; project administration, B.A.; funding acquisition, B.A. All authors have read and agreed to the published version of the manuscript.

## Funding

This work was funded by project grants (PJT165854 and PS173314) from the Canadian Institutes of Health Research to B.A.

## Conflicts of interest

The funders had no role in the design of the study; in the collection, analyses, or interpretation of data; in the writing of

the manuscript; or in the decision to publish the results. B.A. and R.K. are co-inventors on several patents issued worldwide on HKCC adjuvant.

## Data availability

The data supporting the findings in this article will be made available by the authors, without undue reservation, upon reasonable request.

## References

1. Ao D, He X, Liu J, Xu L. Strategies for the development and approval of COVID-19 vaccines and therapeutics in the post-pandemic period. *Signal Transduct Target Ther.* 2023;8:466.
2. Sohrabi C et al. World Health Organization declares global emergency: a review of the 2019 novel coronavirus (COVID-19). *International Journal of Surgery.* 2020;76:71–76.
3. Willyard C. Are repeat COVID infections dangerous? What the science says. *Nature.* 2023;616:650–652.
4. Klaassen F et al. Changes in population immunity against infection and severe disease from severe acute respiratory syndrome coronavirus 2 omicron variants in the United States between December 2021 and November 2022. *Clin Infect Dis.* 2023;77:355–361.
5. Waltz E. China and India approve nasal COVID vaccines—are they a game changer? *Nature.* 2022;609:450.
6. Waltz E. How nasal-spray vaccines could change the pandemic. *Nature.* 2022;609:240–242.
7. Banihashemi SR et al. Safety and efficacy of combined intramuscular/intranasal RAZI-COV PARS vaccine candidate against SARS-CoV-2: a preclinical study in several animal models. *Front Immunol.* 2022;13:836745.
8. Tikhvatulin AI et al. Immunogenicity and protectivity of intranasally delivered vector-based heterologous prime-boost COVID-19 vaccine Sputnik V in mice and non-human primates. *Emerg Microbes Infect.* 2022;11:2229–2247.
9. Kehagia E, Papakyriakopoulou P, Valsami G. Advances in intranasal vaccine delivery: a promising non-invasive route of immunization. *Vaccine.* 2023;41:3589–3603.
10. BenMohamed L, Krishnan R, Auge C, Primus JF, Diamond DJ. Intranasal administration of a synthetic lipopeptide without adjuvant induces systemic immune responses. *Immunology.* 2002; 106:113–121.
11. Hamley IW. Lipopeptides for vaccine development. *Bioconjug Chem.* 2021;32:1472–1490.
12. Tiboni M, Casattari L, Illum L. Nasal vaccination against SARS-CoV-2: Synergistic or alternative to intramuscular vaccines? *Int J Pharm.* 2021;603:120686.
13. Trinité B et al. SARS-CoV-2 infection elicits a rapid neutralizing antibody response that correlates with disease severity. *Sci Rep.* 2021;11:2608.
14. Dispinseri S et al. Neutralizing antibody responses to SARS-CoV-2 in symptomatic COVID-19 is persistent and critical for survival. *Nat Commun.* 2021;12:2670.
15. Riou C et al. Relationship of SARS-CoV-2-specific CD4 response to COVID-19 severity and impact of HIV-1 and tuberculosis coinfection. *J Clin Invest.* 2021;131:
16. Peng Y et al.; ISARIC4C Investigators. Broad and strong memory CD4+ and CD8+ T cells induced by SARS-CoV-2 in UK convalescent individuals following COVID-19. *Nat Immunol.* 2020; 21:1336–1345.
17. Sekine T et al.; Karolinska COVID-19 Study Group. Robust T cell immunity in convalescent individuals with asymptomatic or mild COVID-19. *Cell.* 2020;183:158–168.e14.
18. Peng B, Ming Y, Yang C. Regulatory B cells: the cutting edge of immune tolerance in kidney transplantation review-article. *Cell Death Dis.* 2018;9:109.

19. Heide J et al. Broadly directed SARS-CoV-2-specific CD4+ T cell response includes frequently detected peptide specificities within the membrane and nucleoprotein in patients with acute and resolved COVID-19. *PLoS Pathog.* 2021;17:e1009842.
20. Liu WJ et al. T-cell immunity of SARS-CoV: implications for vaccine development against MERS-CoV. *Antiviral Res.* 2017;137:82–92.
21. Peng H et al. Long-lived memory T lymphocyte responses against SARS coronavirus nucleocapsid protein in SARS-recovered patients. *Virology.* 2006;351:466–475.
22. Meyers LM et al. Highly conserved, non-human-like, and cross-reactive SARS-CoV-2 T cell epitopes for COVID-19 vaccine design and validation. *NPJ Vaccines.* 2021;6:71.
23. Vashi Y, Jagrit V, Kumar S. Understanding the B and T cell epitopes of spike protein of severe acute respiratory syndrome coronavirus-2: a computational way to predict the immunogens. *Infection, Genetics and Evolution.* 2020;84:104382.
24. Tarke A et al. Impact of SARS-CoV-2 variants on the total CD4+ and CD8+ T cell reactivity in infected or vaccinated individuals. *Cell Rep Med.* 2021;2:100355.
25. Li CK et al. T cell responses to whole SARS coronavirus in humans. *J Immunol.* 2008;181:5490–5500.
26. Grifoni A et al. A sequence homology and bioinformatic approach can predict candidate targets for immune responses to SARS-CoV-2. *Cell Host Microbe.* 2020;27:671–680.e2.
27. Liu X et al. Profile of antibodies to the nucleocapsid protein of the Severe Acute Respiratory Syndrome (SARS)-associated coronavirus in probable SARS patients. *Clin Diagn Lab Immunol.* 2004;11:28–31.
28. Wang J et al. Assessment of immunoreactive synthetic peptides from the structural proteins of severe acute respiratory syndrome coronavirus. *Clin Chem.* 2003;49:1989–1996.
29. Patel RS, Agrawal B. Mucosal immunization with lipopeptides derived from conserved regions of SARS-CoV-2 antigens induce robust cellular and cross-variant humoral immune responses in mice. *Front Immunol.* 2023;14:1178523.
30. Gupta N et al. Harnessing innate immunity to treat mycobacterium tuberculosis infections: heat-killed *caulobacter crescentus* as a novel biotherapeutic. *Cells.* 2023;12:560.
31. Thermofisher Corp. BestProtocols: Staining Intracellular Antigens for Flow Cytometry. <https://www.thermofisher.com/ca/en/home/references/protocols/cell-and-tissue-analysis/protocols/staining-intracellular-antigens-flow-cytometry.html>. Accessed February 21, 2024.
32. Chen H et al. Cytokit: a bioconductor package for an integrated mass cytometry data analysis pipeline. *PLoS Comput Biol.* 2016;12:e1005112.
33. Morpheus. <https://software.broadinstitute.org/morpheus>. Accessed March 1, 2023.
34. Beitari S et al. Cross protection to SARS-CoV-2 variants in hamsters with naturally acquired immunity. *Virology.* 2023;20:167.
35. Corman VM et al. Detection of 2019 novel coronavirus (2019-nCoV) by real-time RT-PCR. *Eurosurveillance.* 2020;25:2000045.
36. Gruber AD et al. Standardization of reporting criteria for lung pathology in SARS-CoV-2-infected hamsters: what matters? *Am J Respir Cell Mol Biol.* 2020;63:856–859.
37. Arifin WN, Zahiruddin WM. Sample size calculation in animal studies using resource equation approach. *Malays J Med Sci.* 2017;24:101–105.
38. Feldman J et al. Naive human B cells engage the receptor binding domain of SARS-CoV-2, variants of concern, and related sarbecoviruses. *Sci Immunol.* 2021;6:eabl5842.
39. Shoostari P et al. Correlation analysis of intracellular and secreted cytokines via the generalized integrated mean fluorescence intensity. *Cytometry A.* 2010;77:873–880.
40. Hofmann N, Grossegeisse M, Neumann M, Schaade L, Nitsche A. Evaluation of a commercial ELISA as alternative to plaque reduction neutralization test to detect neutralizing antibodies against SARS-CoV-2. *Sci Rep.* 2022;12:3549.
41. Dangi T et al. Improved control of SARS-CoV-2 by treatment with a nucleocapsid-specific monoclonal antibody. *J Clin Invest.* 2022;132:e162282.
42. Hikono H et al. T-cell memory and recall responses to respiratory virus infections. *Immunol Rev.* 2006;211:119–132.
43. Zar HJ et al. Natural and hybrid immunity following four COVID-19 waves: A prospective cohort study of mothers in South Africa: natural and hybrid immunity in SARS-CoV2. *EClinicalMedicine.* 2022;53:101655.
44. Goel RR et al. Efficient recall of Omicron-reactive B cell memory after a third dose of SARS-CoV-2 mRNA vaccine. *Cell.* 2022;185:1875–1887.e8.
45. Röltgen K et al. Immune imprinting, breadth of variant recognition, and germinal center response in human SARS-CoV-2 infection and vaccination. *Cell.* 2022;185:1025–1040.e14.
46. Kaku CI et al. Recall of preexisting cross-reactive B cell memory after Omicron BA.1 breakthrough infection. *Sci Immunol.* 2022;7:eabq3511.
47. Hoffmann M et al. Effect of hybrid immunity and bivalent booster vaccination on omicron sublineage neutralisation. *Lancet Infect Dis.* 2023;23:25–28.
48. Chu L et al. Immune response to SARS-CoV-2 after a booster of mRNA-1273: an open-label phase 2 trial. *Nat Med.* 2022;28:1042–1049.
49. Lopez-Munoz AD, Kosik I, Holly J, Yewdell JW. Cell surface SARS-CoV-2 nucleocapsid protein modulates innate and adaptive immunity. *Sci Adv.* 2022;8:eabp9770.
50. Notarbartolo S et al. Integrated longitudinal immunophenotypic, transcriptional and repertoire analyses delineate immune responses in COVID-19 patients. *Sci Immunol.* 2021;6:eabg5021.
51. Bergamaschi L et al. Cambridge Institute of Therapeutic Immunology and Infectious Disease-National Institute of Health Research (CITIID-NIHR) COVID BioResource Collaboration Longitudinal analysis reveals that delayed bystander CD8+ T cell activation and early immune pathology distinguish severe COVID-19 from mild disease. *Immunity.* 2021;54:1257–1275.e8.
52. Moss P. The T cell immune response against SARS-CoV-2. *Nat Immunol.* 2022;23:186–193.
53. Swain SL, McKinstry KK, Strutt TM. Expanding roles for CD4 + T cells in immunity to viruses. *Nat Rev Immunol.* 2012;12:136–148.
54. Jo N et al. Impaired CD4+ T cell response in older adults is associated with reduced immunogenicity and reactogenicity of mRNA COVID-19 vaccination. *Nat Aging.* 2023;3:751.
55. Deliyannis G et al. Induction of Long-Term Memory CD8 + T Cells for Recall of Viral Clearing Responses against Influenza Virus. *J Virol.* 2002;76:4212–4221.
56. Moss P. The T cell immune response against SARS-CoV-2. *Nat Immunol.* 2022;23:186–193.
57. Shakiba MH, Gemünd I, Beyer M, Bonaguro L. Lung T cell response in COVID-19. *Front Immunol.* 2023;14:1108716.
58. Le Bert N et al. SARS-CoV-2-specific T cell immunity in cases of COVID-19 and SARS, and uninfected controls. *Nature.* 2020;584:457–462.
59. Shou S et al. Animal models for COVID-19: hamsters, mouse, ferret, mink, tree shrew, and non-human primates. *Front Microbiol.* 2021;12:626553.
60. Zhang C et al. SARS-CoV-2 virus culture, genomic and subgenomic RNA load, and rapid antigen test in experimentally infected Syrian hamsters. *J Virol.* 2022;96:e0103422.
61. Immergluck K et al. Correlation of sars-cov-2 subgenomic rna with antigen detection in nasal midturbinate swab specimens. *Emerg Infect Dis.* 2021;27:2887–2891.
62. Brocato RL et al. Disruption of adaptive immunity enhances disease in SARS-CoV-2-infected Syrian hamsters. *J Virol.* 2020;94:e01683–20.
63. Heitmann JS et al. A COVID-19 peptide vaccine for the induction of SARS-CoV-2 T cell immunity. *Nature.* 2022;601:617–622.

© The Author(s) 2025. Published by Oxford University Press on behalf of The American Association of Immunologists.

This is an Open Access article distributed under the terms of the Creative Commons Attribution-NonCommercial License (<https://creativecommons.org/licenses/by-nc/4.0/>), which permits non-commercial re-use, distribution, and reproduction in any medium, provided the original work is properly cited. For commercial re-use, please contact [journals.permissions@oup.com](mailto:journals.permissions@oup.com)

ImmunoHorizons, 2025, 9, 1–15  
<https://doi.org/10.1093/immhor/vlae011>  
Research Article